AIMS Mathematics

AIMS Mathematics, 11(9): 28161–28201.
DOI: 10.3934/math.20261123
Received: 08 May 2026
Revised: 12 August 2026
Accepted: 19 August 2026
Published: 03 September 2026

https://www.aimspress.com/journal/Math

Research article

A hybrid pied kingfisher optimizer for constrained continuous optimization: application to 3D UAV path planning

Qiaoping Li* and Jiahao Wan

School of Economics, Zhengzhou University of Aeronautics, Zhengzhou 450046, China

* **Correspondence:** Email: liqiaoping1981@126.com.

Abstract: In this paper, we proposed a hybrid pied kingfisher optimizer (HPKO) for constrained continuous optimization and applied it to three-dimensional unmanned aerial vehicle (3D UAV) path planning under terrain and threat constraints. Based on the original pied kingfisher optimizer (PKO), HPKO integrated tent chaotic initialization, refracted opposition-based learning (ROBL), and intelligent boundary control (IBC) to enhance population diversity, local optimum escape, and solution feasibility near variable bounds. HPKO was evaluated on the CEC2017 and CEC2022 benchmark suites and compared with 13 well-known optimization algorithms in terms of solution quality, convergence behavior, robustness, and statistical significance. Results showed that HPKO maintains strong overall competitiveness across search landscapes and dimensional settings. Ablation studies showed that ROBL provides the strongest standalone improvement across the four function categories, while the complete three-module configuration achieved the best overall rank. In the 3D UAV simulations, HPKO achieved the lowest composite cost among HPKO, PKO, PSO, and GWO in simple and complex terrain–threat environments, with a larger margin in the complex scenario. Weight sensitivity analysis further quantified the trade-offs among path length, external threat exposure, and altitude behavior. These results demonstrated that HPKO serves as an effective constrained optimization framework with practical value for 3D UAV path planning.

Keywords: constrained optimization; metaheuristic algorithm; boundary handling; opposition-based learning; 3D UAV path planning
Mathematics Subject Classification: 90C26, 90C59, 68T20

1. Introduction

Constrained continuous optimization arises naturally in three-dimensional unmanned aerial vehicle (UAV) path planning, where candidate trajectories must satisfy terrain-clearance, threat-avoidance, altitude, and maneuverability requirements. Such planning requirements are encountered in last-mile delivery [1], autonomous operation in GPS-denied environments [2], and infrastructure inspection around complex structures [3]. Across these applications, path length, collision risk, flight feasibility, and computational cost are recurrent planning criteria [4]. When a trajectory is parameterized by intermediate waypoints, the resulting optimization problem becomes high-dimensional and multimodal, with a composite nonconvex objective that poses challenges for conventional gradient-based optimization. Terrain and threat constraints may further restrict the feasible region, making diversity preservation and reliable constraint handling central to the search process.

Classical planners remain important in UAV path planning because they exploit graph, geometric, or sampling structures. A survey of multirotor applications summarizes graph-search, sampling-based, and optimization-based approaches [5]. Modified A* has been applied to stealth UAV planning in three-dimensional radar environments [6], whereas bidirectional artificial-potential-field-guided RRT* (APF-RRT*) combines potential-field guidance with goal-biased sampling [7]; direct obstacle-avoidance mechanisms have also been developed for UAV planning [8]. These methods, however, remain sensitive to their design and parameter settings: APF-based motion may exhibit switching and chattering [9], while sampling-based planners depend on step size, goal bias, and post-processing. Beyond route construction, studies have increasingly emphasized trajectory formulation and optimization. Warm-started optimization improves formation-planning efficiency [10], while four-dimensional swarm planning extends the decision space to coordinated temporal motion [11]. A two-stage transport formulation explicitly links decision variables, objectives, and operational constraints in trajectory planning and tracking [12], and mathematical optimization has also been integrated with search-based robotic planning [13]. Collectively, these studies indicate that planner performance depends not only on the search mechanism but also on how application objectives and feasibility constraints are represented.

Optimization methods range from deterministic approaches based on explicit structural assumptions to derivative-free population-based methods for nonconvex search spaces. For structured convex problems, the golden-ratio primal-dual algorithm has established convergence guarantees [14], while its line-search extension permits adaptive step sizes without prior knowledge of the spectral norm of the linear operator [15]. These guarantees, however, rely on convex structure, whereas terrain–threat waypoint planning is generally nonconvex and multimodal, thereby motivating population-based search. Optimization-based UAV planning has been reviewed across algorithm families [16]. Representative studies improve flower pollination through neighborhood-global learning [17], augment the artificial gorilla troops optimizer with mutation and interpolation [18], incorporate safety mechanisms into spherical-vector particle swarm optimization [19], and combine grey wolf optimization with chaos-game search [20]. A multi-strategy bottlenose dolphin optimizer provides a further example of coordinating several search operators for UAV planning [21]. Related optimization mechanisms have also been applied to conflict-free automated-guided-vehicle coordination [22], heterogeneous-task scheduling [23], mobile-robot localization [24], engineering design [25], and parameter identification under uncertainty [26]. Although these studies expand the available search mechanisms and application settings, constrained waypoint planning requires an effective balance between preserving population diversity and maintaining candidate feasibility.

Optimization studies increasingly combine learning, metaheuristic, and decomposition mechanisms according to the structure of the problem being addressed. In adaptive reinforcement learning control, the slime mould algorithm has been used to adjust the learning rate of proximal policy optimization during training [27]. Moreover, a molecular fuzzy decision framework integrates information gain, Q-learning, genetic weighting, and multi-objective particle swarm optimization across stages of the decision process [28]. For mixed discrete-continuous optimization in a space-air-ground integrated network, deep Q-learning is combined with an alternating-optimization decomposition scheme, with Differential Annealing employed to solve the resulting subproblems [29]. These studies highlight the value of assigning each component a clearly defined function within an integrated solution process.

The pied kingfisher optimizer (PKO) represents perching or hovering, diving, and symbiotic foraging as exploration, exploitation, and information-exchange phases, respectively [30]. Its multi-phase structure has supported a range of extensions for numerical and engineering optimization. EPKO was developed as an enhanced PKO variant for benchmark and engineering problems [31], while other PKO-based methods have been applied to proton-exchange-membrane fuel-cell parameter extraction [32], attribute reduction [33], and numerical and engineering optimization [34]. These studies demonstrate the adaptability of the PKO framework across problem settings. However, the separate and coordinated roles of initial population coverage, diversity recovery, and boundary handling remain insufficiently examined in constrained search.

Three algorithmic limitations motivate the proposed design. First, purely random initialization may yield uneven search-space coverage and limited initial population diversity. Second, as the search proceeds, the PKO population may become concentrated around locally promising but suboptimal regions, increasing the risk of stagnation. Third, exploratory updates may generate out-of-bound candidates, whereas simple clipping or random resetting may discard useful directional information. These considerations call for a modular design whose components can be evaluated separately and whose integrated behavior can be examined in constrained UAV path planning.

To address these limitations, we propose a hybrid pied kingfisher optimizer (HPKO) as a modular extension of PKO. Tent chaotic initialization (CTI) is introduced to improve initial search-space coverage and population diversity. Multi-elite refracted opposition-based learning (ROBL) combines a middle-stage branch activated by stagnation or low population diversity with a late-stage elite-guided opposition branch to recover diversity during the search. Intelligent boundary control (IBC) maps out-of-bound candidates back into the bounded search domain through periodic reflection and violation-dependent, direction-preserving shrinkage toward the current best solution. The three modules can be activated independently, enabling their individual and combined effects to be examined through ablation analysis. Their integrated applicability is further illustrated in a constrained three-dimensional UAV path-planning scenario.

The major contributions of this study are summarized as follows:

(1) A modular Hybrid Pied Kingfisher Optimizer, termed HPKO, is proposed for constrained continuous optimization. HPKO integrates CTI, state- and stage-conditioned multi-elite ROBL, and IBC to improve initial search-space coverage, recover population diversity under stagnation, and repair out-of-bound candidates while preserving useful search directions. The three modules can be activated independently, enabling their individual and combined effects to be examined within a unified framework.

(2) A theoretical and numerical evaluation framework is established for HPKO. Under a bounded search domain and a lower-bounded objective function, the historical population-best objective sequence is shown to converge to a finite limit through greedy selection and best-solution preservation.

HPKO is further evaluated on the CEC2017 and CEC2022 benchmark suites against 13 conventional, recent, and PKO-related optimization algorithms through comparative tests, empirical convergence analysis, nonparametric statistical tests, effect-size analysis, and module-level ablation. These analyses assess solution quality, stability, and the individual and combined roles of the three enhancement modules.

(3) HPKO is applied to three-dimensional UAV path planning under terrain and cylindrical-threat constraints. The path-planning model integrates hard terrain-clearance and threat-exclusion requirements with path length, buffered threat exposure, altitude preference, and maneuverability costs. Comparisons with PKO, PSO, and GWO in simple and complex environments, together with weight sensitivity analysis, show that HPKO achieves the lowest composite cost in both scenarios, with a more pronounced advantage in the complex environment.

The remainder of this paper is organized as follows: In Section 2, we formulate the UAV path-planning problem. In Section 3, we describe PKO and HPKO. In Section 4, we present the benchmark tests and analyses. In Section 5, we report the UAV simulations. In Section 6, we conclude the paper and outline future work.

2. Problem formulation of 3D UAV path planning

2.1. Environment model

The UAV operates in a three-dimensional mission space $\Omega \subset \mathbb{R}^3$ with horizontal coordinates (x, y) and terrain elevation $z(x, y)$. To represent large-scale undulations and localized terrain features while maintaining a simple and reproducible terrain model, the elevation field is expressed as the superposition of a smooth base surface and a set of Gaussian hills:

$$z(x, y) = z_b(x, y) + \sum_{i=1}^{N_g} z_{p,i}(x, y). \tag{1}$$

The base terrain $z_b(x, y)$ is modeled by a compact trigonometric mixture capturing low-frequency undulations:

$$z_b(x, y) = a_1 \sin(b_1 x)\cos(c_1 y) + a_2 \sin(b_2 x)\sin(c_2 y) + a_3 \cos(b_3 x)\cos(c_3 y), \tag{2}$$

where the coefficients control the overall roughness and spatial frequency of the terrain undulations, and are fixed across all simulation scenarios.

Localized terrain features are represented by Gaussian hills:

$$z_{p,i}(x, y) = h_i \exp\left(-\frac{(x-x_i)^2}{2\sigma_{x,i}^2} - \frac{(y-y_i)^2}{2\sigma_{y,i}^2}\right), i = 1, \dots, N_g, \tag{3}$$

where (x_i, y_i) denotes the horizontal location of the i-th peak and h_i is its peak height. Parameters $\sigma_{x,i}, \sigma_{y,i}$ are horizontal spread parameters along the east–west and north–south directions, respectively, which determine how rapidly the elevation decays away from (x_i, y_i). By adjusting the number of peaks and their parameters, the superposed terrain $z(x, y)$ can represent simple environments with a few gentle hills and complex environments with multiple steep mountains.

2.2. Threat model and flight constraints

In addition to the static terrain, the UAV must avoid threat regions such as radar stations or anti-aircraft positions. Each threat is represented as a vertical cylinder

$$\mathcal{T}_j = \left\{(x, y, z) \mid \left(x - x_j^{th}\right)^2 + \left(y - y_j^{th}\right)^2 \leq R_j^2, z \leq H_j^{th}\right\}, j = 1, \dots, N_t, \tag{4}$$

where (x_j^{th}, y_j^{th}) is the horizontal position of the j-th threat source, R_j is its effective horizontal detection radius, and H_j^{th} is the altitude up to which the threat is active. The union of all such cylinders $\mathcal{T} = \bigcup_{j=1}^{N_t} \mathcal{T}_j$ defines the hard exclusion zones that the planned path must avoid.

The UAV path is represented as a sequence of $N + 1$ waypoints

$$\mathbf{P}_k = [x_k, y_k, z_k]^\top, k = 0, 1, \dots, N, \tag{5}$$

where $\mathbf{P}_0$ and $\mathbf{P}_N$ denote the fixed start and goal positions, and the intermediate waypoints $\mathbf{P}_1, \dots, \mathbf{P}_{N-1}$ are optimization variables. The corresponding decision vector is formed by stacking all waypoint coordinates into a $3(N - 1)$-dimensional vector.

To ensure feasibility and flight safety, the following constraints are imposed on the trajectory.

(1) Minimum segment length.

The Euclidean distance between two consecutive waypoints

$$\ell_k = \|\mathbf{P}_{k+1} - \mathbf{P}_k\|_2, k = 0, \dots, N - 1, \ell_k \geq \ell_{\min}, \tag{6}$$

where $\ell_{\min}$ is a predefined minimum segment length that avoids excessive waypoint density. In our simulations, a fixed number of waypoints is adopted, and this constraint is not activated (equivalently setting $\ell_{\min} = 0$); it is included for completeness and can be enabled when dense waypoint layouts must be avoided.

(2) Turn angle and climb angle constraints.

Let $\mathbf{v}_k = \mathbf{P}_k - \mathbf{P}_{k-1}$ denote the direction vector of the k-th segment. The horizontal turn angle at waypoint k is defined as

$$\psi_k = \angle(\mathbf{v}_k^{xy}, \mathbf{v}_{k+1}^{xy}), \tag{7}$$

where $\mathbf{v}_k^{xy}$ is the projection of $\mathbf{v}_k$ onto the x–y plane. The vertical climb angle of segment k is

$$\theta_k = \arctan \frac{z_{k+1} - z_k}{\|\mathbf{P}_{k+1}^{xy} - \mathbf{P}_k^{xy}\|_2}. \tag{8}$$

To respect the UAV's maneuverability and aerodynamic limits, the constraints

$$|\psi_k| \leq \psi_{\max}, |\theta_k| \leq \theta_{\max} \tag{9}$$

are handled via hinge-type penalties in the objective function, i.e., penalties are activated only when $|\psi_k| > \psi_{\max}$ or $|\theta_k| > \theta_{\max}$, which discourages aggressive maneuvers while keeping the search numerically stable.

(3) Flight altitude constraints.

For terrain following and flight safety, the altitude of each waypoint must satisfy the terrain-clearance constraint:

$$z_k \geq z(x_k, y_k) + h_{clr}, k = 0, \dots, N, \tag{10}$$

where h_{clr} is the prescribed terrain-clearance margin. The preferred maximum flight altitude $h_{\max}$ is treated as a soft limit, and exceedance of this limit is penalized through the altitude cost defined in Eqs (15) and (16).

Within the optimization framework considered in this study, the coordinate bounds of the decision vector are enforced by the IBC operator described in Section 3.4. Terrain clearance and threat avoidance determine path feasibility, whereas the preferred altitude ceiling enters the objective through the altitude penalty defined in Eqs (15) and (16), and the maneuverability limits are incorporated through the smoothness term in Eq (17).

2.3. Path cost functions

The objective of 3D path planning is to determine a waypoint sequence that satisfies safety constraints while minimizing an overall performance index reflecting route efficiency and flight quality. A feasibility-first evaluation is adopted, in which candidates violating terrain-clearance or threat-avoidance constraints are assigned a large penalty. For feasible trajectories, the total cost is computed from four terms representing path length, external threat exposure, altitude preference, and path smoothness.

2.3.1. Path length cost

The path length cost is defined as the sum of Euclidean distances between consecutive waypoints:

$$J_{\text{len}} = \sum_{k=0}^{N-1} \ell_k = \sum_{k=0}^{N-1} \|\mathbf{P}_{k+1} - \mathbf{P}_k\|_2. \tag{11}$$

A shorter path typically reduces travel distance and is often associated with lower flight time and energy usage when other mission settings are comparable.

2.3.2. Threat cost

To quantify safety with respect to threat regions, we adopt a feasibility-first threat-handling scheme consistent with the cylindrical threat model in (4). For each threat T_j with center (x_j^{th}, y_j^{th}), radius R_j, and active height H_j^{th}, a trajectory point (x, y, z) violates the threat constraint if

$$\left(x - x_j^{th}\right)^2 + \left(y - y_j^{th}\right)^2 \leq R_j^2 \; and \; z \leq H_j^{th}. \tag{12}$$

To evaluate the complete trajectory, each segment between consecutive waypoints is uniformly sampled. If any sampled point satisfies the threat-intersection condition in (12), the candidate path is declared infeasible and assigned $J_{\text{INF}} = 10^8$. For a feasible path, the threat cost is evaluated within a fixed external buffer around each cylindrical threat region. Let

$$\mathbf{P}_k(t) = (1 - t)\mathbf{P}_k + t\mathbf{P}_{k+1}, 0 \leq t \leq 1, \tag{13}$$

and let $d_j\left(\mathbf{P}_k(t)\right)$ denote the horizontal distance from $\mathbf{P}_k(t)$ to the center of threat T_j, and $\chi_j(t)$ is the altitude-activation indicator, with $\chi_j(t)$=1 when $z_k(t) \leq H_j^{th}$ and $\chi_j(t)$=0 otherwise. The threat-exposure cost is defined as

$$J_{\text{thr}} = \begin{cases} \sum_{k=0}^{N-1} L_k \int_0^1 \sum_{j=1}^{N_t} \chi_j(t) \left[\max(0,1 - \frac{d_j(\mathbf{P}_k(t)) - R_j}{b_{th}})\right]^2, & \text{if the path is threat-feasible,} \\ J_{\text{INF}}, & \text{otherwise.} \end{cases} \quad (14)$$

Here, ℓ_k is the length of segment k, and $b_{\text{th}} = 5$ m is the external buffer width. The integral is approximated using the uniformly sampled points along each segment. The cylindrical threat regions remain hard exclusion zones, while the threat term differentiates feasible paths according to their clearance from the threat boundaries.

2.3.3. Altitude cost

Although the flight altitude is bounded by mission/airspace limits, it is also desirable to maintain sufficient terrain clearance while avoiding unnecessarily high-altitude detours. Let $z(x_k, y_k)$ denote the terrain elevation at waypoint $\mathbf{P}_k$, and let h_{clr} be the prescribed clearance margin. Let $h_{\min}(k) = z(x_k, y_k) + h_{clr}$ denote the minimum safe altitude at waypoint $\mathbf{P}_k$.

The altitude cost is defined as

$$J_{\text{alt}} = \sum_{k=0}^{N} \psi_h(z_k, h_{\min}(k)), \quad (15)$$

where $\psi_h(\cdot)$ is a penalty function.

$$\psi_h(z_k, h_{\min}(k)) = \begin{cases} 0, & h_{\min}(k) \le z_k \le h_{\max}, \\ (z_k - h_{\max})^2, & z_k > h_{\max}, \\ J_{\text{INF}}, & z_k < h_{\min}(k). \end{cases} \quad (16)$$

This term assigns an infeasibility penalty below the minimum safe altitude and penalizes exceedance of the preferred altitude ceiling.

2.3.4. Path smoothness cost

For flight stability and control performance, the path should avoid abrupt changes in direction and altitude. A smoothness cost is therefore introduced based on violations of the prescribed turn- and climb-angle limits:

$$J_{\text{sm}} = \sum_{k=1}^{N-1} \{\alpha_\psi [\max(0, |\psi_k| - \psi_{max})]^2 + \alpha_\theta [\max(0, |\theta_k| - \theta_{max})]^2\}, \quad (17)$$

where α_ψ and α_θ are weighting coefficients. This hinge-squared form activates penalties only when the maneuver limits are violated; hence, J_{sm}=0 for trajectories satisfying both limits.

2.3.5. Composite cost function

Finally, the overall path-planning problem is solved using a feasibility-first evaluation. Any candidate trajectory that violates safety-critical constraints (terrain clearance and threat avoidance) is treated as infeasible and assigned a large penalty. For feasible trajectories, the objective is computed as a weighted sum of efficiency and flight-quality terms:

$$\min_{\{\mathbf{P}_1, \dots, \mathbf{P}_{N-1}\}} J = w_1 J_{\text{len}} + w_2 J_{\text{thr}} + w_3 J_{\text{alt}} + w_4 J_{\text{sm}}, \quad (18)$$

where $w_1, \dots, w_4$ are nonnegative weights assigned to path length, external threat exposure, altitude preference, and path smoothness, respectively. Accordingly, the coordinates of the intermediate waypoints in (5) form the $D = 3(N-1)$-dimensional decision vector used in the optimization, and the composite cost in (18) is used as the corresponding fitness function.

3. Proposed HPKO algorithm

In this section, we first review the basic PKO and then present the three enhancement modules of the proposed HPKO: Tent chaotic initialization, multi-elite refracted opposition-based learning, and intelligent boundary control. The integrated procedure is subsequently summarized through pseudocode and a flowchart, followed by convergence and computational complexity analyses.

3.1. *Pied kingfisher optimizer*

PKO is a swarm intelligence algorithm that represents the perching or hovering, diving, and symbiotic foraging behaviors of pied kingfishers through distinct search phases [30]. The corresponding update mechanisms are described below.

3.1.1. Population representation and initialization

In PKO, each kingfisher corresponds to a candidate solution in a D-dimensional search space. Let

$$\mathbf{x}_i^t = [x_{i1}^t, x_{i2}^t, \dots, x_{iD}^t]^\top, \quad i = 1,2,\dots,N_p, \tag{19}$$

denote the position of the i-th kingfisher at iteration t, where N_p is the population size; for the UAV path-planning problem, $\mathbf{x}_i^t$ stacks the coordinates of the $N-1$ intermediate waypoints in (5), and hence $D = 3(N-1)$.

$$\mathbf{L} = [L_1, L_2, \dots, L_D]^\top, \quad \mathbf{U} = [U_1, U_2, \dots, U_D]^\top, \tag{20}$$

where $\mathbf{L}$ and $\mathbf{U}$ denote the lower- and upper-bound vectors, respectively. The original PKO generates the initial population uniformly at random:

$$x_{id}^0 = L_d + r_{id}(U_d - L_d), \quad r_{id} \sim \mathcal{U}(0,1), \quad d = 1,2,\dots,D. \tag{21}$$

Each individual is evaluated by the objective function $f(\mathbf{x}_i^t)$, and the global best solution is recorded as $\mathbf{x}_{\text{best}}^t$ with fitness f_{best}^t.

3.1.2. Exploration phase (perching and hovering)

At each iteration, a kingfisher decides whether to explore or dive according to a Bernoulli trial. For the i-th individual, a random number $r \sim \mathcal{U}(0,1)$ is drawn; if $r < 0.8$ the individual performs exploration, otherwise it enters the diving phase.

In the exploration phase, PKO abstracts two behaviors observed in nature: perching and hovering. Both can be written in the generic form.

$$\mathbf{x}_i^{t+1} = \mathbf{x}_i^t + s^t \boldsymbol{\xi}_i^t \odot (\mathbf{x}_j^t - \mathbf{x}_i^t), \tag{22}$$

where $j \neq i$, $\boldsymbol{\xi}_i^t$ is a random vector whose components are independently generated, and s^t is a time-varying step-size factor.

In the perching mode, s^t is a relatively large step length modulated by a cosine function of a random feather angle, which enables wide-range movements guided by promising individuals.

In the hovering mode, s^t is scaled by a beating-rate term related to the fitness ratio $\mathrm{Fit}(j)/\mathrm{Fit}(i)$ and by the iteration ratio $t/T_{\max}$, so that fitter individuals perform more intensive local search in high-quality regions.

By switching between these two behaviors, PKO conducts multi-scale exploration while progressively biasing the population toward high-fitness regions.

3.1.3. Exploitation phase (diving)

When $r \geq 0.8$, the kingfisher engages in a diving behavior that drives the solution toward the current global best. A typical diving update can be expressed as

$$\mathbf{x}_i^{t+1} = \mathbf{x}_i^t + \sigma^t \beta_i^t (\mathbf{x}_{\text{best}}^t - \mathbf{x}_i^t), \tag{23}$$

where $\beta_i^t \sim \mathcal{N}(0,1)$ is a Gaussian perturbation and σ^t is a decaying contraction factor, usually defined as a decreasing function of $t/T_{\max}$. In the early stage, larger values of σ^t enable relatively coarse movements toward $\mathbf{x}_{\text{best}}^t$, whereas in the late stage, small σ^t values enable fine-grained refinement around the current best solution.

3.1.4. Symbiotic phase

In addition to individual behaviors, PKO models a symbiotic phase that reflects mutualistic cooperation between kingfishers and other animals. Pairs of individuals exchange information to refine their positions:

$$\mathbf{x}_i^{t+1} = \mathbf{x}_i^t + H^t (\mathbf{x}_j^t - \mathbf{x}_k^t), \tag{24}$$

where j and k are indices of two randomly selected individuals, and H^t is a hunting-efficiency coefficient, often defined as a linearly increasing function

$$H^t = H_{\min} + (H_{\max} - H_{\min}) \frac{t}{T_{\max}}. \tag{25}$$

The symbiotic phase enriches the search dynamics by allowing information exchange between regions of the search space, which helps balance exploration and exploitation.

3.2. Tent chaotic initialization

The distribution of the initial population affects the subsequent search behavior of PKO. If the initial individuals are concentrated within a limited region, the available population diversity may be reduced. To alleviate this problem, HPKO employs Tent chaotic initialization to promote more even coverage of the search space.

Let $u_{id}^{(k)} \in [0,1]$ denote the chaotic state associated with the i-th individual and the d-th dimension at iteration k of the chaotic map. The Tent map is defined as

$$u_{id}^{(k+1)} = \begin{cases} \frac{u_{id}^{(k)}}{\gamma}, & 0 \le u_{id}^{(k)} < \gamma, \\ \frac{1-u_{id}^{(k)}}{1-\gamma}, & \gamma \le u_{id}^{(k)} \le 1, \end{cases} \tag{26}$$

where $\gamma \in (0,1)$ is a control parameter, usually set to $\gamma = 0.5$ to obtain good ergodicity. Starting from a random seed $u_{id}^{(0)} \sim \mathcal{U}(0,1)$ and iterating the Tent map several steps, a chaotic sequence $u_{id}^{(k)}$ is generated.

The chaotic variables are then linearly mapped to the actual search space:

$$x_{id}^{0} = L_d + u_{id}^{(K)}(U_d - L_d), \tag{27}$$

where K is the number of Tent iterations performed before mapping. In this study, K = 100 is used to reduce the direct dependence of the mapped population on the initial random states. The resulting initialization is intended to improve initial search-space coverage and population diversity relative to purely random initialization.

3.3. *Multi-elite refracted opposition-based learning*

To mitigate premature convergence and help the algorithm escape local optima, HPKO incorporates a two-branch refracted opposition-based learning (ROBL) strategy. The state-triggered branch combines classical opposition points with refracted points guided by the current global best.

Given the lower and upper bounds $\mathbf{L}$ and $\mathbf{U}$, the classical opposite of $\mathbf{x}_i^t$ is defined as

$$\mathbf{x}_i^{\mathrm{op}} = \mathbf{L} + \mathbf{U} - \mathbf{x}_i^t. \tag{28}$$

Using the current global best $\mathbf{x}_{\mathrm{best}}^t$ as a reference, a refracted opposite point is constructed as

$$\mathbf{x}_i^{\mathrm{rf}}(t) = \mathbf{x}_{\mathrm{best}}^t + \eta(t)(\mathbf{x}_i^{\mathrm{op}} - \mathbf{x}_{best}^t), \tag{29}$$

where $\eta(t)$ is a refractive coefficient that decreases with the iteration index so that ROBL performs larger jumps in earlier iterations and more conservative perturbations later.

ROBL is activated when the search exhibits stagnation or when the population diversity becomes low. A group of relatively poor individuals is then selected. For each selected individual, HPKO considers three candidates, $\mathbf{x}_i^t, \mathbf{x}_i^{\mathrm{op}}, \mathbf{x}_i^{\mathrm{rf}}(t)$, applies IBC to enforce the coordinate bounds (Section 3.4), and retains the one with the lowest cost:

$$\mathbf{x}_i^{t+1} = \arg \min_{z \in \{\mathbf{x}_i^t, \mathbf{x}_i^{\mathrm{op}}, \mathbf{x}_i^{\mathrm{rf}}(t)\}} f(\boldsymbol{z}). \tag{30}$$

During the later search stage, a multi-elite branch further uses elite solutions to guide the refinement of inferior individuals. By selectively introducing refracted opposite candidates, ROBL broadens the available search directions around promising regions and reduces the risk of premature stagnation.

3.4. Intelligent boundary control

The decision vector is subject to the coordinate-wise bounds in (20), which are enforced by IBC after each candidate update. Simple clipping

$$\tilde{x}_{id} = \min(\max(x_{id}, L_d), U_d) \tag{31}$$

may cause individuals to accumulate at the boundaries and induce oscillatory behavior. To better handle boundary violations, HPKO employs an intelligent boundary control (IBC) operator that combines periodic reflection with direction-preserving shrinkage.

Let $\mathbf{y}$ be a candidate solution generated by a PKO update. For each dimension d, define the span $S_d = U_d - L_d$. The first step is periodic reflection:

$$\hat{y}_d = L_d + \mathrm{mod}(|y_d - L_d|, 2S_d), \tag{32}$$

followed by folding back into the feasible interval:

$$y_d^{\mathrm{ref}} = \begin{cases} \hat{y}_d, & \hat{y}_d \le U_d \\ 2U_d - \hat{y}_d, & \hat{y}_d > U_d. \end{cases} \tag{33}$$

This operation is equivalent to repeatedly reflecting the point at the borders until it lies in $[L_d, U_d]$, avoiding the saturation effect of simple truncation.

To further reduce large excursions near the boundary, a direction-preserving shrinkage is applied toward the current global best solution $\mathbf{x}_{\mathrm{best}}^t$:

$$\mathbf{y}^{\mathrm{new}} = \mathbf{y}^{\mathrm{ref}} + \kappa(\mathbf{x}_{\mathrm{best}}^{\mathrm{t}} - \mathbf{y}^{\mathrm{ref}}), \tag{34}$$

where the shrinkage factor κ is adaptively determined based on the severity of the boundary violation. Specifically, let $v_d = \max(0, L_d - y_d, y_d - U_d)$ denote the violation magnitude in dimension d, and $S_d = U_d - L_d$ the corresponding search span. The normalized violation is then $\hat{v}_d = v_d / S_d$. To ensure stronger correction for severe violations while preserving mild adjustments for near-boundary points, we define

$$\kappa = min(\kappa_{max}, \tfrac{1}{D}\textstyle\sum_{d=1}^{D} \hat{v}_d), \tag{35}$$

where $\kappa_{max} = 0.9$ is an upper bound to prevent over-shrinking, and D is the problem dimension. In this way, severely violating candidates are pulled closer to $\mathbf{x}_{\mathrm{best}}^t$, while mildly violating ones are only slightly adjusted. Since the direction from $\mathbf{x}_{\mathrm{best}}^t$ to $\mathbf{y}^{\mathrm{ref}}$ is preserved, IBC preserves the useful search direction while satisfying the coordinate bounds.

The computational procedure of HPKO is summarized in Algorithm 1, and the overall workflow is illustrated in Figure 1.

Algorithm 1. Pseudocode of HPKO.

```
Inputs: Objective function f, population size Np, problem dimension D,
  maximum number of iterations Tmax, bounds L and U, and parameter settings
Output: Best solution xbest and its objective value fbest

Initialize the population using Tent chaotic initialization in (26) and (27)
Evaluate all individuals and determine xbest and fbest
Set t = 1
while t ≤ Tmax do
for i = 1 to Np do
Generate a candidate yi using the PKO updates in (22)–(24)
Apply IBC to yi according to (31)–(35)
Evaluate f(yi) and perform greedy selection
end for
Update xbest and fbest
Update the ROBL controls and check the state- or stage-based activation condition
if ROBL is activated then
Select inferior individuals according to the active ROBL branch
for each selected individual xj do
Generate the opposite and refracted candidates using (28) and (29)
Apply IBC to the generated candidates and evaluate their fitness
Retain the best candidate according to (30)
end for
Update xbest and fbest
end if
Set t = t + 1
end while
Return xbest and fbest
```

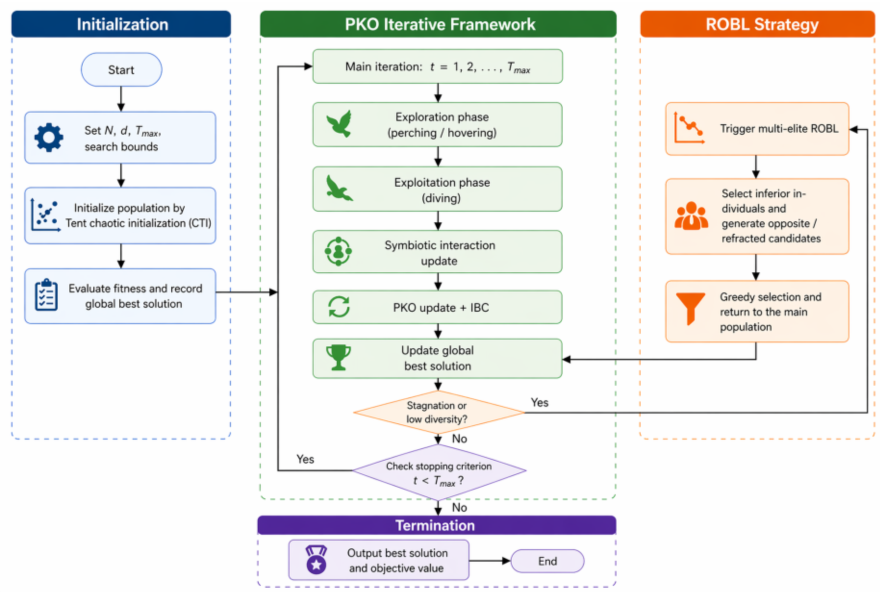

Figure 1. The flowchart of HPKO.

3.5. Convergence and computational complexity analysis

HPKO is developed within the population-based stochastic search framework of the original PKO, with CTI, ROBL, and IBC introduced to improve population diversity, local-optimum escape, and boundary handling. Since the stochastic operators do not impose deterministic descent on every population member, the convergence analysis focuses on the population-best objective sequence under greedy selection and best-solution preservation. Let

$$f_{\mathrm{best}}^{t} = \min_{1 \le i \le N_p} f(\mathbf{x}_i^t) \tag{36}$$

denote the best objective value in the population at iteration *t*. Suppose that the search domain $\mathcal{X} = \{\mathbf{x} \in \mathbb{R}^{\mathrm{D}} \mid \mathbf{L} \le \mathbf{x} \le \mathbf{U}\}$ is bounded and that f is bounded below on $\mathcal{X}$. The IBC operator maps each out-of-bound candidate back into $\mathcal{X}$, so all accepted solutions remain within the bounded search domain. In addition, HPKO applies strict greedy selection and preserves the historical global-best solution. It therefore follows that $f_{\mathrm{best}}^{t+1} \le f_{\mathrm{best}}^{t}, t = 0,1,\dots,T_{\max} - 1$.

Thus, $\{f_{\mathrm{best}}^{t}\}$ is a monotone non-increasing sequence bounded from below and therefore converges to a finite limiting value. This result establishes convergence of the population-best objective sequence under the stated conditions, but does not imply convergence to the global optimum. The practical convergence behavior of HPKO is further examined through the CEC benchmark curves in Section 4 and the UAV path-planning curves in Section 5. In both studies, the convergence curves track the best-so-far sequence defined in (36), with the objective evaluated by the corresponding CEC test function and the composite UAV path cost in (18), respectively.

The computational complexity of HPKO is mainly determined by the original PKO updates and the additional overhead introduced by the three enhancement modules. Let N_p denote the population size, D the problem dimension, $T_{\max}$ the maximum number of iterations, and C_f the cost of one fitness evaluation. In the original PKO, each iteration consists of population updating and fitness evaluation, leading to an overall complexity of $O\big(T_{\max}N_p(D + C_f)\big)$. For HPKO, Tent chaotic initialization is executed only once before the iterative search and thus introduces only a one-time preprocessing cost. The intelligent boundary control operator is applied after each PKO update and adds a linear repair cost with respect to the population size and problem dimension. The ROBL strategy is conditionally activated and operates on a subset of individuals, so its additional overhead is limited to selected iterations rather than the whole optimization process. Therefore, the dominant computational cost of HPKO comes from the original PKO iteration and fitness evaluation, and its overall computational complexity remains $O\big(T_{\max}N_p(D + C_f)\big)$.

4. Numerical analysis

In this section, we present a comprehensive numerical analysis to evaluate the effectiveness of the proposed HPKO and to clarify the specific roles of its three enhancement modules. First, the computational environment, benchmark suites, compared algorithms, and parameter settings were described to establish a fair and reproducible evaluation protocol. Then, ablation tests were conducted to isolate the individual and joint contributions of the three modules, thereby clarifying whether the observed performance gains arose from a single dominant strategy or from their coordinated integration. Subsequently, HPKO was evaluated on the CEC2017 and CEC2022 benchmark suites from the perspectives of solution quality and convergence behavior to examine its performance across heterogeneous search landscapes and different dimensional settings. Statistical tests were incorporated into the ablation and comparative analyses to assess whether the observed performance differences were reliable rather than incidental.

4.1. Computational environment and test settings

All benchmark tests were conducted on a desktop computer running Windows 11, equipped with an Intel Core i5 processor and 16 GB of RAM. To ensure a fair comparison, all algorithms were evaluated under the same test protocol, using the same population size, iteration budget, and number of independent runs. Specifically, the population size was fixed at 50, the maximum number of iterations was set to 1000, and each algorithm was independently executed 30 times on every test function.

4.1.1. Benchmark test functions

To evaluate the performance of HPKO on diverse continuous optimization landscapes, two representative benchmark suites, namely CEC2017 and CEC2022, were employed in this study. The CEC2017 suite was tested at 30, 50, and 100 dimensions, whereas the CEC2022 suite was tested at 10 and 20 dimensions. Across these settings, the benchmark functions covered unimodal, multimodal, hybrid, and composition categories, thereby providing a broad testbed for examining exploitation accuracy, exploration capability, and robustness under different search difficulties. Following the official CEC2017 guidelines, function F2 was excluded from the present tests owing to its unstable behavior in high-dimensional spaces. The detailed benchmark functions used in this study are listed in Tables 1 and 2.

Table 1. CEC2017 test functions used in this study.

Type	ID	CEC2017 function name	Range	Dimension	fmin
Unimodal	F1	Shifted and rotated bent cigar function	[-100,100]	30/50/100	100
	F3	Shifted and rotated Zakharov function	[-100,100]	30/50/100	300
Multimodal	F4	Shifted and rotated Rosenbrock's function	[-100,100]	30/50/100	400
	F5	Shifted and rotated Rastrigin's function	[-100,100]	30/50/100	500
	F6	Shifted and rotated Expanded Scaffer's F6 function	[-100,100]	30/50/100	600
	F7	Shifted and rotated Lunacek Bi-Rastrigin function	[-100,100]	30/50/100	700
	F8	Shifted and rotated non-continuous Rastrigin's function	[-100,100]	30/50/100	800
	F9	Shifted and rotated Levy function	[-100,100]	30/50/100	900
	F10	Shifted and rotated Schwefel's function	[-100,100]	30/50/100	1000
Hybrid	F11	Hybrid function 1 (N = 3)	[-100,100]	30/50/100	1100
	F12	Hybrid function 2 (N = 3)	[-100,100]	30/50/100	1200
	F13	Hybrid function 3 (N = 3)	[-100,100]	30/50/100	1300
	F14	Hybrid function 4 (N = 4)	[-100,100]	30/50/100	1400
	F15	Hybrid function 5 (N = 4)	[-100,100]	30/50/100	1500
	F16	Hybrid function 6 (N = 4)	[-100,100]	30/50/100	1600
	F17	Hybrid function 7 (N = 5)	[-100,100]	30/50/100	1700

Continued on next page

Type	ID	CEC2017 function name	Range	Dimension	fmin
Hybrid	F18	Hybrid function 8 (N = 5)	[-100,100]	30/50/100	1800
	F19	Hybrid function 9 (N = 5)	[-100,100]	30/50/100	1900
	F20	Hybrid function 10 (N = 6)	[-100,100]	30/50/100	2000
Composition	F21	Composition function 1 (N = 3)	[-100,100]	30/50/100	2100
	F22	Composition function 2 (N = 3)	[-100,100]	30/50/100	2200
	F23	Composition function 3 (N = 4)	[-100,100]	30/50/100	2300
	F24	Composition function 4 (N = 4)	[-100,100]	30/50/100	2400
	F25	Composition function 5 (N = 5)	[-100,100]	30/50/100	2500
	F26	Composition function 6 (N = 5)	[-100,100]	30/50/100	2600
	F27	Composition function 7 (N = 6)	[-100,100]	30/50/100	2700
	F28	Composition function 8 (N = 6)	[-100,100]	30/50/100	2800
	F29	Composition function 9 (N = 3)	[-100,100]	30/50/100	2900
	F30	Composition function 10 (N = 3)	[-100,100]	30/50/100	3000

Table 2. CEC2022 test functions used in this study.

Type	ID	CEC2022 function name	Range	Dimension	fmin
Unimodal	F1	Shifted and full rotated Zakharov function	[-100,100]	10/20	300
Multimodal	F2	Shifted and rotated Rosenbrock's function	[-100,100]	10/20	400
	F3	Shifted and full rotated Expanded Schaffer's F7 function	[-100,100]	10/20	600
Hybrid	F4	Shifted and rotated non-continuous Rastrigin's function	[-100,100]	10/20	800
	F5	Shifted and rotated Levy function	[-100,100]	10/20	900
	F6	Hybrid function 1	[-100,100]	10/20	1800
	F7	Hybrid function 2	[-100,100]	10/20	2000
	F8	Hybrid function 3	[-100,100]	10/20	2200
Composition	F9	Composition function 1	[-100,100]	10/20	2300
	F10	Composition function 2	[-100,100]	10/20	2400
	F11	Composition function 3	[-100,100]	10/20	2600
	F12	Composition function 4	[-100,100]	10/20	2700

4.1.2. Comparative algorithms and parameter settings

To provide a comparative evaluation that is readable and sufficiently representative, HPKO was benchmarked against 13 optimization algorithms selected from four categories: PKO-related algorithms, classical reference algorithms, recent competitive algorithms, and recent multi-strategy algorithms. This classification clarified the comparative roles of the algorithm groups and enabled direct assessment against the original PKO, its enhanced variant EPKO, established optimizers, and proposed metaheuristics with different search characteristics.

PKO-related algorithms. This category includes the original PKO and the enhanced variant EPKO.

Classical reference algorithms. These include Particle Swarm Optimization (PSO), Differential Evolution (DE), Grey Wolf Optimizer (GWO), and Simulated Annealing (SA).

Recent competitive algorithms. These include Dream Optimization Algorithm (DOA), Dung Beetle Optimizer (DBO), Kangaroo Escape Optimizer (KEO), Traffic Jam Optimizer (TJO), and Educational Competition Optimizer (ECO).

Recent multi-strategy algorithms. These include Transient Trigonometric Harris Hawks Optimizer (TTHHO) and Black Widow Optimization with a Gaussian mutation algorithm (BWOG).

For all compared algorithms, the common test protocol described in Section 4.1 was adopted. The fixed control parameters of each algorithm were determined according to the corresponding literature or public implementations and remained unchanged across all benchmark functions, whereas stochastic quantities were generated during execution according to the original update mechanisms. All parameter settings and implementation choices were fixed before the formal tests, and the reported parameter values were adopted as uniform default settings without function-specific tuning. The major parameter settings of HPKO and the compared algorithms are summarized in Table 3.

Table 3. Major parameter settings of HPKO and the compared algorithms.

Algorithm	Main parameter settings
HPKO	BF = 8; PEmax = 0.5; PEmin = 0; κmax = 0.9
PKO	BF = 8; PEmax = 0.5; PEmin = 0
EPKO	BF = 8; PEmax = 0.5; PEmin = 0; β = 1.5; simplex = 1, 2, 0.5, 0.5; nworst = 5
DOA	Five groups; exploration/exploitation stages = 0.9T/0.1T; p = 0.9
PSO	wmax = 0.9; wmin = 0.4; c1 = c2 = 2.0
DE	F = 0.5; CR = 0.9
GWO	a decrease linearly from 2 to 0
SA	T0 = 50; cooling rate = 0.85
DBO	k = 0.1; b = 0.3; S = 0.5
KEO	Energy threshold = 0.5; zigzag scale factor β = 0.5
TJO	a = [0.5,1.5], c = [1.5,0.5]
ECO	H = 0.5; G1 = 0.2N; G2 = 0.1N
TTHHO	E0 ∈ [-1,1]; r ∈ [0,1]; σ = 1.5; a = 2
BWOG	pc = 0.8; pC = 0.5; pM = 0.4

4.2. Ablation study

To examine the individual and combined effects of the three enhancement modules, an ablation study was conducted on the CEC2017 benchmark suite. The suite contained 29 functions spanning unimodal, multimodal, hybrid, and composition categories, providing a suitable basis for module-level comparison. Five variants were considered: the original PKO, CTI-PKO, ROBL-PKO, IBC-PKO, and the full HPKO. CTI-PKO, ROBL-PKO, and IBC-PKO were obtained by activating one enhancement module at a time while keeping all other settings unchanged. Each variant was independently executed 30 times on all 29 functions. For each function, the mean best-fitness value over the 30 runs was used to rank the five variants, and the average rank across all functions was used for the overall comparison. Sign tests and Wilcoxon signed-rank tests based on the function-wise mean values were also conducted between HPKO and each of the other variants.

The overall ablation results are summarized in Table 4. Compared with the original PKO, all three single-module variants achieve lower average ranks, although the extent of improvement differs. Among them, ROBL-PKO performs best, reducing the average rank from 4.45 to 2.00 and ranking first on four functions. This result identifies ROBL as the strongest standalone enhancement under the present test setting. The full HPKO achieves the lowest average rank of 1.17 and ranks first on 24 of the 29 functions, showing that the integrated framework provides the best overall configuration. Pairwise sign and Wilcoxon signed-rank tests further indicate significant differences in favor of HPKO over PKO and the three single-module variants ($p < 0.001$), suggesting that the combined use of CTI, ROBL, and IBC provides additional improvement beyond the individual modules.

Table 4. Overall ablation results of the five variants on CEC2017.

Variant	Average rank ↓	First-place functions	Wins vs HPKO	Losses vs HPKO	Sign test p	Wilcoxon p
PKO	4.45	0	0	29	3.73E-09	2.56E-06
CTI-PKO	4.38	0	0	29	3.73E-09	2.56E-06
ROBL-PKO	2.00	4	4	25	1.04E-04	2.47E-04
IBC-PKO	3.00	1	1	28	1.12E-07	5.32E-06
HPKO	**1.17**	24	—	—	—	—

Note: Wins and losses are counted relative to HPKO using function-wise mean values; lower average ranks indicate better performance.

To further examine the performance of the three modules across function categories, the average ranks of the five variants are reported by function group in Table 5. HPKO obtains the best grouped average rank on the multimodal, hybrid, and composition functions and shares the best rank with ROBL-PKO on the unimodal functions. Among the single-module variants, ROBL-PKO ranks best in all four categories. These grouped results identify ROBL as the strongest standalone module, while the lower ranks achieved by the full HPKO on three of the four categories show that the complete three-module configuration provides further improvement.

Table 5. Grouped average ranks of the ablation variants on CEC2017.

Function group	No. of functions	PKO	CTI-PKO	ROBL-PKO	IBC-PKO	HPKO
Unimodal	2	4.00	4.50	1.50	3.50	**1.50**
Multimodal	7	4.43	4.57	2.14	2.86	**1.00**
Hybrid	10	4.60	4.40	2.10	2.80	**1.10**
Composition	10	4.40	4.20	1.90	3.20	**1.30**

Figure 2 presents the function-wise rank profiles of the five variants. HPKO lies closest to the center on most functions, consistent with its 24 first-place results in Table 4. ROBL-PKO generally follows HPKO, whereas PKO and CTI-PKO occupy the outer rank regions on more functions. The figure therefore provides a visual summary of the overall and grouped rankings reported in Tables 4 and 5.

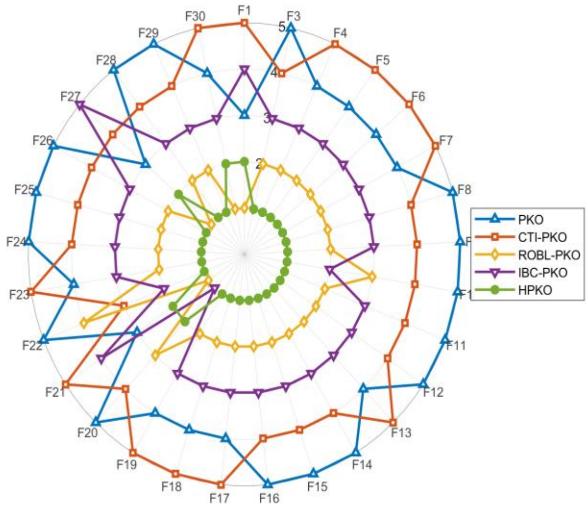

Figure 2. Function-wise rank profiles of the five ablation variants on CEC2017.

In summary, the ablation study leads to three major observations. First, each enhancement module improves the average rank of the original PKO under the common test setting. Second, ROBL provides the strongest standalone improvement and achieves the best single-module rank in every function category. Third, the full HPKO achieves the best overall rank and leads or ties across the four function categories. The statistical tests further show that HPKO outperforms PKO and the three single-module variants, indicating that the complete configuration provides additional improvement over the individual modules. In the next subsection, we evaluate HPKO against the external optimizers on the CEC2017 and CEC2022 benchmark suites.

4.3. Comparative results on the CEC2017 and CEC2022 benchmark suites

4.3.1. Results on the CEC2017 benchmark suite

Comparative tests were conducted on the CEC2017 benchmark suite at 30, 50, and 100 dimensions. The results were analyzed in terms of function-wise solution quality, overall rankings, pairwise statistical comparisons, and representative convergence behavior.

Table 6 presents the results for CEC2017 at 30D. HPKO obtains the lowest average Friedman rank of 1.483, followed by EPKO and DOA with ranks of 2.655 and 3.207, respectively. At the function level, HPKO achieves the lowest mean values on most multimodal and hybrid functions and on several composition functions, contributing to the best overall ranking across the 30-dimensional suite.

The 50-dimensional results are presented in Table 7. HPKO obtains the lowest average Friedman rank of 1.862, followed by DOA and EPKO, and maintains the leading suite-level position at 50D.

Table 8 reports the results at 100D. HPKO again ranks first, with an average Friedman rank of 1.759, while DOA and EPKO rank second and third, respectively. Together with the results at 30D and 50D, the 100-dimensional results show that HPKO maintains the lowest suite-level rank across the three tested dimensional settings.

Table 6. Statistical results of HPKO and competing algorithms on CEC2017 (30D).

Function	Statistic	**HPKO**	PKO	EPKO	DOA	PSO	DE	GWO	SA	DBO	KEO	TJO	ECO	TTHHO	BWOG
F1	Mean	**1.001E+02**	2.637E+06	5.393E+02	5.360E+03	8.817E+08	9.991E+03	1.573E+09	6.949E+03	8.792E+06	4.108E+03	1.399E+03	1.880E+07	3.266E+07	2.794E+08
	Std	**1.822E-01**	4.375E+06	5.062E+02	4.407E+03	1.142E+09	5.323E+03	1.359E+09	6.282E+03	1.248E+07	4.192E+03	1.129E+03	2.348E+07	9.197E+06	1.483E+08
F3	Mean	3.673E+02	9.836E+04	**3.000E+02**	2.785E+04	1.802E+04	1.342E+05	4.553E+04	1.564E+05	7.114E+04	4.184E+03	9.312E+03	2.878E+04	3.972E+04	4.289E+04
	Std	7.325E+01	2.854E+04	**1.182E-04**	1.463E+04	8.177E+03	1.782E+04	1.194E+04	5.349E+04	1.357E+04	1.954E+03	3.052E+03	7.201E+03	8.174E+03	1.172E+04
F4	Mean	4.868E+02	5.032E+02	**4.296E+02**	4.730E+02	5.821E+02	4.969E+02	5.922E+02	5.068E+02	5.499E+02	4.854E+02	5.051E+02	5.310E+02	5.724E+02	5.743E+02
	Std	5.710E+00	2.256E+01	**2.912E+01**	2.438E+01	1.114E+02	9.033E+00	1.123E+02	3.960E+01	5.367E+01	3.840E+01	1.561E+01	2.574E+01	5.004E+01	2.701E+01
F5	Mean	**5.448E+02**	5.873E+02	5.699E+02	5.529E+02	5.780E+02	6.671E+02	6.124E+02	6.320E+02	7.075E+02	6.089E+02	6.264E+02	6.964E+02	7.391E+02	6.110E+02
	Std	**1.526E+01**	2.553E+01	1.590E+01	1.257E+01	2.036E+01	8.556E+00	4.247E+01	3.264E+01	4.676E+01	2.707E+01	2.070E+01	4.830E+01	3.992E+01	1.463E+01
F6	Mean	**6.000E+02**	6.031E+02	6.001E+02	**6.000E+02**	6.032E+02	**6.000E+02**	6.076E+02	**6.000E+02**	6.361E+02	6.177E+02	6.241E+02	6.465E+02	6.652E+02	6.176E+02
	Std	**4.123E-05**	4.004E+00	1.434E-01	**1.938E-02**	2.180E+00	**1.221E-04**	2.748E+00	**2.363E-03**	1.160E+01	9.876E+00	5.630E+00	9.070E+00	7.583E+00	4.214E+00
F7	Mean	**7.702E+02**	8.425E+02	8.149E+02	7.924E+02	8.232E+02	9.009E+02	8.699E+02	8.804E+02	9.422E+02	9.114E+02	8.324E+02	1.062E+03	1.298E+03	8.431E+02
	Std	**1.417E+01**	3.652E+01	2.042E+01	1.495E+01	3.557E+01	9.509E+00	4.905E+01	3.525E+01	6.927E+01	3.777E+01	2.401E+01	1.002E+02	7.463E+01	2.108E+01
F8	Mean	**8.488E+02**	8.867E+02	8.587E+02	8.608E+02	8.717E+02	9.639E+02	8.966E+02	9.335E+02	1.007E+03	9.012E+02	9.063E+02	9.492E+02	9.742E+02	8.908E+02
	Std	**1.459E+01**	2.908E+01	1.150E+01	9.826E+00	1.456E+01	1.157E+01	2.984E+01	3.233E+01	4.664E+01	2.726E+01	2.356E+01	3.165E+01	2.078E+01	1.590E+01
F9	Mean	**9.001E+02**	1.387E+03	9.337E+02	1.078E+03	1.080E+03	1.026E+03	1.843E+03	5.863E+03	5.263E+03	2.145E+03	1.686E+03	4.788E+03	8.282E+03	1.757E+03
	Std	**1.273E-01**	8.448E+02	4.519E+01	1.608E+02	2.166E+02	5.537E+01	6.381E+02	1.941E+03	2.402E+03	5.000E+02	4.589E+02	9.300E+02	9.001E+02	2.752E+02
F10	Mean	4.496E+03	4.867E+03	4.842E+03	**3.288E+03**	4.269E+03	7.094E+03	4.506E+03	4.390E+03	5.296E+03	4.924E+03	5.395E+03	5.603E+03	6.209E+03	4.524E+03
	Std	5.489E+02	7.352E+02	5.325E+02	**3.472E+02**	6.785E+02	2.918E+02	1.158E+03	5.588E+02	7.218E+02	6.899E+02	9.677E+02	6.497E+02	8.848E+02	5.301E+02
F11	Mean	**1.140E+03**	1.262E+03	1.179E+03	1.148E+03	1.290E+03	1.354E+03	2.061E+03	1.743E+03	1.499E+03	1.244E+03	1.233E+03	1.287E+03	1.319E+03	1.766E+03
	Std	**2.974E+01**	4.565E+01	3.294E+01	3.063E+01	7.985E+01	4.042E+01	1.134E+03	6.900E+02	1.386E+02	5.745E+01	3.902E+01	6.193E+01	5.726E+01	2.756E+02
F12	Mean	**1.943E+04**	2.252E+06	2.422E+04	9.731E+05	1.112E+08	1.622E+07	6.379E+07	3.056E+06	2.418E+07	6.776E+05	4.526E+06	5.397E+06	3.717E+07	2.352E+07
	Std	**1.472E+04**	1.829E+06	1.186E+04	1.333E+06	3.239E+08	7.421E+06	7.944E+07	1.945E+06	2.986E+07	6.632E+05	2.495E+06	3.566E+06	3.880E+07	1.396E+07
F13	Mean	**2.291E+03**	4.517E+04	7.451E+03	3.578E+03	5.564E+06	1.068E+06	2.731E+05	2.561E+04	5.263E+06	1.819E+04	3.622E+04	4.216E+04	7.522E+05	7.874E+06
	Std	**1.761E+03**	3.317E+04	5.039E+03	3.047E+03	1.805E+07	8.043E+05	9.399E+05	2.608E+04	1.038E+07	1.571E+04	1.190E+04	4.139E+04	3.655E+05	1.190E+07

Continued on next page

Function	Statistic	**HPKO**	PKO	EPKO	DOA	PSO	DE	GWO	SA	DBO	KEO	TJO	ECO	TTHHO	BWOG
F14	Mean	**1.444E+03**	4.398E+04	1.549E+03	1.276E+05	4.809E+04	1.705E+05	4.172E+05	1.880E+06	7.024E+04	6.344E+03	1.122E+04	5.949E+04	6.844E+05	2.605E+05
	Std	**1.106E+01**	4.398E+04	5.030E+01	1.365E+05	6.254E+04	1.038E+05	7.700E+05	1.945E+06	7.909E+04	6.119E+03	1.492E+04	6.705E+04	6.577E+05	1.964E+05
F15	Mean	**1.541E+03**	3.366E+04	2.460E+03	3.398E+03	2.320E+04	2.170E+05	5.765E+05	2.375E+04	9.603E+04	9.404E+03	1.650E+04	1.925E+04	9.766E+04	6.566E+03
	Std	**2.863E+01**	1.515E+04	1.035E+03	2.781E+03	3.069E+04	1.500E+05	1.031E+06	1.495E+04	8.985E+04	8.454E+03	6.968E+03	1.616E+04	4.340E+04	5.274E+03
F16	Mean	**2.047E+03**	2.402E+03	2.377E+03	2.330E+03	2.466E+03	2.578E+03	2.594E+03	2.881E+03	3.152E+03	2.540E+03	2.652E+03	2.723E+03	3.574E+03	2.617E+03
	Std	**2.076E+02**	2.944E+02	2.324E+02	1.911E+02	2.585E+02	1.440E+02	3.767E+02	3.498E+02	3.268E+02	3.402E+02	2.645E+02	3.639E+02	4.355E+02	2.392E+02
F17	Mean	**1.839E+03**	1.994E+03	1.935E+03	1.965E+03	2.064E+03	2.031E+03	1.983E+03	2.440E+03	2.528E+03	2.182E+03	2.009E+03	2.308E+03	2.651E+03	2.079E+03
	Std	**9.375E+01**	1.142E+02	9.318E+01	1.351E+02	1.781E+02	8.384E+01	1.527E+02	2.075E+02	2.745E+02	2.152E+02	1.200E+02	2.469E+02	2.763E+02	1.531E+02
F18	Mean	1.878E+04	5.429E+05	**2.875E+03**	2.803E+05	9.526E+05	1.487E+06	1.491E+06	4.400E+06	1.923E+06	9.562E+04	1.418E+05	4.605E+05	1.792E+06	5.304E+05
	Std	1.703E+04	4.264E+05	**7.289E+02**	1.634E+05	1.183E+06	7.949E+05	1.655E+06	3.983E+06	2.891E+06	1.242E+05	7.643E+04	3.946E+05	2.116E+06	4.956E+05
F19	Mean	**1.922E+03**	3.383E+04	5.672E+03	2.626E+03	3.558E+04	1.615E+05	7.302E+05	2.428E+04	6.538E+05	7.740E+03	6.133E+05	1.662E+04	1.298E+06	3.266E+04
	Std	**8.674E+00**	2.057E+04	3.163E+03	9.503E+02	5.439E+04	1.355E+05	8.488E+05	1.986E+04	1.955E+06	9.269E+03	3.638E+05	1.598E+04	9.961E+05	3.630E+04
F20	Mean	**2.146E+03**	2.347E+03	2.269E+03	2.312E+03	2.324E+03	2.329E+03	2.457E+03	2.619E+03	2.681E+03	2.525E+03	2.418E+03	2.545E+03	2.772E+03	2.294E+03
	Std	**9.857E+01**	1.657E+02	8.935E+01	1.730E+02	1.485E+02	9.209E+01	1.700E+02	1.610E+02	2.173E+02	2.365E+02	9.814E+01	1.751E+02	2.200E+02	6.669E+01
F21	Mean	**2.344E+03**	2.376E+03	2.357E+03	2.356E+03	2.378E+03	2.464E+03	2.389E+03	2.440E+03	2.526E+03	2.390E+03	2.398E+03	2.473E+03	2.579E+03	2.408E+03
	Std	**1.302E+01**	2.076E+01	1.352E+01	1.095E+01	1.820E+01	1.085E+01	2.473E+01	2.940E+01	3.707E+01	1.959E+01	2.155E+01	6.465E+01	5.112E+01	1.912E+01
F22	Mean	**2.300E+03**	5.820E+03	3.433E+03	3.538E+03	3.612E+03	4.657E+03	4.431E+03	5.782E+03	5.289E+03	4.251E+03	2.302E+03	4.775E+03	6.225E+03	2.489E+03
	Std	**1.230E-12**	1.541E+03	1.804E+03	1.288E+03	1.671E+03	1.077E+03	1.753E+03	4.909E+02	2.101E+03	2.019E+03	1.702E+00	2.542E+03	2.199E+03	7.371E+01
F23	Mean	**2.703E+03**	2.730E+03	2.713E+03	2.710E+03	2.856E+03	2.814E+03	2.751E+03	2.774E+03	2.909E+03	2.768E+03	2.771E+03	2.871E+03	3.196E+03	2.810E+03
	Std	**1.619E+01**	2.027E+01	1.400E+01	1.193E+01	5.940E+01	1.176E+01	3.626E+01	2.264E+01	6.282E+01	3.827E+01	3.401E+01	7.619E+01	1.429E+02	3.184E+01
F24	Mean	**2.866E+03**	2.907E+03	2.875E+03	2.906E+03	3.028E+03	3.014E+03	2.945E+03	2.980E+03	3.085E+03	2.921E+03	2.916E+03	3.066E+03	3.377E+03	2.942E+03
	Std	**1.323E+01**	2.323E+01	1.487E+01	2.237E+01	5.517E+01	1.133E+01	5.736E+01	4.440E+01	5.679E+01	2.603E+01	2.671E+01	8.231E+01	1.494E+02	2.899E+01
F25	Mean	2.887E+03	2.903E+03	2.888E+03	**2.886E+03**	2.910E+03	2.888E+03	2.981E+03	2.894E+03	2.945E+03	2.896E+03	2.945E+03	2.921E+03	2.948E+03	3.004E+03
	Std	1.821E-01	3.143E+01	2.104E+00	**1.800E+00**	3.093E+01	3.191E-01	4.453E+01	1.400E+01	4.796E+01	1.356E+01	1.804E+01	2.265E+01	2.875E+01	3.125E+01
F26	Mean	4.066E+03	4.528E+03	4.362E+03	3.635E+03	4.573E+03	5.277E+03	4.669E+03	5.093E+03	6.179E+03	4.953E+03	**3.594E+03**	5.691E+03	7.837E+03	5.540E+03
	Std	1.490E+02	2.648E+02	2.044E+02	7.243E+02	9.887E+02	1.114E+02	4.459E+02	3.081E+02	8.970E+02	5.419E+02	**1.228E+03**	1.216E+03	1.038E+03	1.229E+03
F27	Mean	3.203E+03	3.212E+03	3.214E+03	3.216E+03	3.267E+03	3.220E+03	3.252E+03	3.233E+03	3.280E+03	3.238E+03	3.286E+03	3.276E+03	3.471E+03	**3.200E+03**

Continued on next page

Function	Statistic	**HPKO**	PKO	EPKO	DOA	PSO	DE	GWO	SA	DBO	KEO	TJO	ECO	TTHHO	BWOG
	Std	6.152E+00	8.585E+00	7.613E+00	4.842E+00	4.359E+01	3.314E+00	2.139E+01	1.845E+01	3.947E+01	1.934E+01	3.011E+01	3.433E+01	1.455E+02	**2.777E-04**
F28	Mean	3.208E+03	3.275E+03	**3.177E+03**	3.208E+03	3.313E+03	3.263E+03	3.444E+03	3.253E+03	3.419E+03	3.226E+03	3.242E+03	3.307E+03	3.348E+03	3.296E+03
	Std	2.842E+01	3.662E+01	**5.669E+01**	1.269E+01	6.329E+01	1.824E+01	1.156E+02	4.398E+01	3.447E+02	2.322E+01	2.382E+01	3.267E+01	3.521E+01	3.171E+00
F29	Mean	**3.461E+03**	3.692E+03	3.567E+03	3.536E+03	3.682E+03	3.903E+03	3.863E+03	3.956E+03	4.251E+03	3.959E+03	4.116E+03	4.419E+03	4.926E+03	4.139E+03
	Std	**6.771E+01**	1.798E+02	1.040E+02	1.027E+02	2.524E+02	1.420E+02	2.151E+02	2.389E+02	2.673E+02	2.672E+02	1.924E+02	3.884E+02	5.909E+02	2.047E+02
F30	Mean	7.216E+03	4.442E+04	**6.192E+03**	9.113E+03	1.396E+05	1.050E+05	8.130E+06	1.508E+04	2.560E+06	1.211E+04	2.703E+06	1.645E+05	6.493E+06	2.430E+06
	Std	1.567E+03	3.268E+04	**7.839E+02**	2.607E+03	2.171E+05	4.394E+04	5.232E+06	4.532E+03	3.506E+06	5.157E+03	1.379E+06	1.484E+05	7.825E+06	1.035E+06
Average rank		**1.483**	6.448	2.655	3.207	7.655	8.655	9.655	8.862	11.793	6.276	7.069	9.931	12.793	8.517

Note: F2 was omitted. Bold values indicate the best mean for each function. The last row reports the average Friedman rank (lower is better).

Table 7. Statistical results of HPKO and competing algorithms on CEC2017 (50D).

Function	Statistic	**HPKO**	PKO	EPKO	DOA	PSO	DE	GWO	SA	DBO	KEO	TJO	ECO	TTHHO	BWOG
F1	Mean	6.252E+03	9.180E+07	**2.658E+03**	8.654E+04	3.176E+09	5.316E+06	8.877E+09	1.584E+04	4.220E+08	3.931E+03	1.456E+04	1.470E+09	3.476E+08	5.062E+08
	Std	7.155E+03	1.227E+08	**3.250E+03**	2.608E+04	2.713E+09	6.317E+06	4.324E+09	1.211E+04	2.560E+08	3.920E+03	4.481E+03	1.215E+09	2.550E+08	3.034E+08
F3	Mean	2.839E+04	2.719E+05	**6.687E+02**	1.378E+05	1.291E+05	2.988E+05	1.087E+05	3.777E+05	2.113E+05	4.976E+04	2.234E+04	1.167E+05	1.279E+05	1.257E+05
	Std	7.378E+03	5.621E+04	**3.476E+02**	2.145E+04	3.203E+04	3.362E+04	1.756E+04	6.538E+04	4.857E+04	1.665E+04	4.892E+03	3.131E+04	2.018E+04	1.151E+04
F4	Mean	5.394E+02	6.438E+02	**4.854E+02**	5.169E+02	8.734E+02	6.322E+02	9.443E+02	5.691E+02	1.135E+03	5.809E+02	5.945E+02	8.082E+02	8.566E+02	7.415E+02
	Std	4.894E+01	4.548E+01	**4.650E+01**	4.471E+01	2.821E+02	2.858E+01	1.712E+02	5.742E+01	1.637E+03	6.041E+01	4.366E+01	1.295E+02	1.042E+02	5.704E+01
F5	Mean	**5.877E+02**	7.350E+02	7.087E+02	6.182E+02	6.670E+02	8.838E+02	7.161E+02	7.593E+02	9.451E+02	7.334E+02	7.528E+02	8.434E+02	9.144E+02	7.023E+02
	Std	**2.210E+01**	5.421E+01	2.903E+01	2.145E+01	3.626E+01	1.863E+01	3.676E+01	4.046E+01	9.423E+01	4.189E+01	4.437E+01	3.399E+01	2.638E+01	2.011E+01
F6	Mean	**6.000E+02**	6.110E+02	6.045E+02	6.003E+02	6.102E+02	6.001E+02	6.212E+02	**6.000E+02**	6.547E+02	6.333E+02	6.358E+02	6.611E+02	6.763E+02	6.217E+02
	Std	**4.281E-03**	1.015E+01	4.708E+00	1.119E-01	4.801E+00	1.500E-02	4.326E+00	**2.830E-02**	1.127E+01	7.085E+00	9.019E+00	6.203E+00	3.647E+00	4.146E+00
F7	Mean	**8.367E+02**	1.058E+03	1.028E+03	8.921E+02	1.007E+03	1.149E+03	1.061E+03	1.048E+03	1.257E+03	1.187E+03	9.974E+02	1.530E+03	1.873E+03	1.004E+03
	Std	**3.350E+01**	8.467E+01	4.501E+01	2.234E+01	7.971E+01	1.795E+01	6.360E+01	4.597E+01	1.228E+02	1.009E+02	6.311E+01	1.486E+02	9.455E+01	3.044E+01
F8	Mean	**8.911E+02**	1.021E+03	9.848E+02	9.212E+02	9.649E+02	1.187E+03	1.033E+03	1.048E+03	1.274E+03	1.052E+03	1.050E+03	1.127E+03	1.221E+03	1.012E+03

Continued on next page

Function	Statistic	**HPKO**	PKO	EPKO	DOA	PSO	DE	GWO	SA	DBO	KEO	TJO	ECO	TTHHO	BWOG
	Std	**3.197E+01**	5.694E+01	3.258E+01	1.993E+01	3.843E+01	1.833E+01	5.765E+01	4.234E+01	9.939E+01	4.444E+01	3.492E+01	5.560E+01	4.076E+01	2.147E+01
F9	Mean	**9.038E+02**	4.603E+03	2.723E+03	3.176E+03	4.010E+03	4.233E+03	7.137E+03	1.481E+04	1.783E+04	6.970E+03	6.182E+03	1.558E+04	2.910E+04	5.138E+03
	Std	**2.786E+00**	4.177E+03	9.169E+02	1.600E+03	2.258E+03	7.118E+02	3.099E+03	5.794E+03	7.315E+03	1.483E+03	2.650E+03	2.136E+03	3.513E+03	1.052E+03
F10	Mean	7.379E+03	8.354E+03	9.024E+03	**5.408E+03**	7.400E+03	1.353E+04	8.114E+03	6.804E+03	9.836E+03	8.275E+03	7.870E+03	8.946E+03	9.910E+03	7.183E+03
	Std	8.294E+02	8.919E+02	7.196E+02	**4.479E+02**	9.327E+02	4.969E+02	2.359E+03	7.046E+02	1.361E+03	1.126E+03	8.484E+02	1.510E+03	9.235E+02	7.059E+02
F11	Mean	**1.188E+03**	2.017E+03	1.284E+03	1.237E+03	1.496E+03	2.766E+03	5.168E+03	7.408E+03	2.046E+03	1.363E+03	1.387E+03	1.731E+03	1.812E+03	1.900E+03
	Std	**3.119E+01**	3.361E+02	4.143E+01	4.429E+01	2.633E+02	3.991E+02	2.149E+03	6.674E+03	2.812E+02	6.265E+01	5.098E+01	2.439E+02	1.204E+02	8.125E+02
F12	Mean	4.399E+05	3.799E+07	**3.981E+05**	5.848E+06	1.044E+09	2.628E+08	6.506E+08	1.475E+07	4.167E+08	5.236E+06	2.110E+07	8.231E+07	2.966E+08	1.430E+08
	Std	3.280E+05	3.337E+07	**3.017E+05**	3.153E+06	1.386E+09	9.117E+07	5.808E+08	7.836E+06	3.697E+08	3.208E+06	9.560E+06	6.661E+07	1.557E+08	7.787E+07
F13	Mean	9.676E+03	1.666E+05	3.416E+03	**3.381E+03**	3.764E+08	3.703E+06	1.403E+08	2.141E+04	9.655E+06	1.486E+04	5.226E+04	6.829E+05	7.923E+06	1.113E+08
	Std	7.787E+03	1.664E+05	1.960E+03	**1.662E+03**	6.082E+08	3.052E+06	1.331E+08	1.424E+04	1.351E+07	8.478E+03	1.992E+04	6.556E+05	1.098E+07	6.940E+07
F14	Mean	3.595E+03	7.191E+05	**1.807E+03**	5.402E+05	4.421E+05	1.679E+06	7.814E+05	3.323E+06	2.339E+06	8.151E+04	7.758E+04	3.734E+05	4.503E+06	2.306E+06
	Std	2.283E+03	4.095E+05	**1.298E+02**	5.157E+05	7.915E+05	9.830E+05	8.968E+05	4.154E+06	3.068E+06	6.519E+04	4.211E+04	2.145E+05	4.401E+06	1.332E+06
F15	Mean	3.736E+03	5.942E+04	**3.449E+03**	3.633E+03	2.407E+06	5.153E+05	8.022E+06	2.174E+04	4.264E+06	9.389E+03	2.277E+04	5.067E+04	9.761E+05	8.716E+06
	Std	2.274E+03	3.726E+04	**1.471E+03**	3.256E+03	1.300E+07	3.893E+05	2.014E+07	1.114E+04	1.271E+07	5.445E+03	1.022E+04	7.451E+04	1.215E+06	8.495E+06
F16	Mean	**2.775E+03**	3.312E+03	2.996E+03	2.992E+03	3.224E+03	4.386E+03	3.362E+03	3.761E+03	4.363E+03	3.322E+03	3.168E+03	3.680E+03	4.591E+03	2.947E+03
	Std	**3.877E+02**	4.679E+02	2.843E+02	2.726E+02	4.945E+02	1.814E+02	4.999E+02	5.307E+02	6.342E+02	4.610E+02	4.063E+02	5.355E+02	6.187E+02	3.281E+02
F17	Mean	**2.566E+03**	3.049E+03	2.716E+03	2.661E+03	3.070E+03	3.247E+03	2.878E+03	3.325E+03	3.984E+03	3.022E+03	3.199E+03	3.505E+03	3.787E+03	2.889E+03
	Std	**2.168E+02**	2.283E+02	2.037E+02	2.532E+02	2.969E+02	1.361E+02	3.091E+02	3.401E+02	3.941E+02	3.028E+02	2.708E+02	3.766E+02	3.896E+02	1.972E+02
F18	Mean	1.033E+05	2.150E+06	**2.339E+04**	1.895E+06	2.885E+06	8.887E+06	6.208E+06	8.074E+06	5.774E+06	3.232E+05	1.460E+06	2.432E+06	5.990E+06	8.990E+06
	Std	6.347E+04	1.151E+06	**1.431E+04**	1.476E+06	2.659E+06	4.193E+06	7.173E+06	7.838E+06	7.538E+06	2.625E+05	8.291E+05	2.415E+06	7.046E+06	4.649E+06
F19	Mean	**2.730E+03**	8.720E+03	1.259E+04	5.170E+03	6.714E+05	1.684E+05	3.549E+06	1.608E+04	4.122E+06	1.824E+04	1.013E+06	5.705E+04	1.737E+06	1.920E+05
	Std	**1.619E+03**	7.344E+03	4.213E+03	3.366E+03	1.249E+06	1.097E+05	7.213E+06	1.725E+04	6.053E+06	1.156E+04	8.617E+05	7.142E+04	1.399E+06	2.661E+05
F20	Mean	2.776E+03	3.071E+03	2.792E+03	2.750E+03	2.899E+03	3.365E+03	3.019E+03	3.517E+03	3.573E+03	3.266E+03	3.064E+03	3.240E+03	3.523E+03	**2.722E+03**
	Std	2.444E+02	2.984E+02	2.065E+02	2.316E+02	2.893E+02	1.629E+02	4.479E+02	3.040E+02	2.771E+02	3.029E+02	3.076E+02	3.269E+02	3.173E+02	**2.200E+02**
F21	Mean	**2.380E+03**	2.502E+03	2.478E+03	2.424E+03	2.499E+03	2.699E+03	2.507E+03	2.571E+03	2.787E+03	2.505E+03	2.494E+03	2.683E+03	2.902E+03	2.493E+03
	Std	**1.738E+01**	6.845E+01	2.411E+01	1.559E+01	3.185E+01	1.394E+01	2.434E+01	4.709E+01	8.315E+01	3.310E+01	2.938E+01	7.601E+01	7.627E+01	2.594E+01

Continued on next page

Function	Statistic	**HPKO**	PKO	EPKO	DOA	PSO	DE	GWO	SA	DBO	KEO	TJO	ECO	TTHHO	BWOG
F22	Mean	8.973E+03	1.030E+04	1.047E+04	**7.007E+03**	8.951E+03	1.529E+04	9.517E+03	8.645E+03	1.126E+04	9.539E+03	8.264E+03	1.087E+04	1.171E+04	8.019E+03
	Std	8.739E+02	6.508E+02	8.145E+02	**1.085E+03**	1.340E+03	4.041E+02	2.123E+03	8.446E+02	1.568E+03	9.512E+02	3.179E+03	1.233E+03	8.509E+02	3.098E+03
F23	Mean	**2.824E+03**	2.954E+03	2.927E+03	2.860E+03	3.237E+03	3.119E+03	2.972E+03	3.018E+03	3.401E+03	2.991E+03	2.991E+03	3.266E+03	3.928E+03	3.064E+03
	Std	**3.292E+01**	5.749E+01	3.446E+01	1.773E+01	9.645E+01	1.399E+01	6.235E+01	5.105E+01	1.307E+02	6.189E+01	4.923E+01	1.247E+02	2.181E+02	4.714E+01
F24	Mean	**2.987E+03**	3.071E+03	3.074E+03	3.081E+03	3.395E+03	3.322E+03	3.165E+03	3.241E+03	3.461E+03	3.124E+03	3.137E+03	3.496E+03	4.270E+03	3.169E+03
	Std	**2.681E+01**	4.839E+01	2.439E+01	3.933E+01	9.714E+01	1.485E+01	1.063E+02	6.063E+01	1.283E+02	5.797E+01	4.791E+01	1.566E+02	3.009E+02	3.811E+01
F25	Mean	**3.024E+03**	3.154E+03	3.066E+03	3.038E+03	3.155E+03	3.060E+03	3.592E+03	3.063E+03	3.497E+03	3.099E+03	3.111E+03	3.283E+03	3.282E+03	3.226E+03
	Std	**2.920E+01**	5.056E+01	2.760E+01	1.840E+01	1.239E+02	1.380E+01	1.956E+02	2.558E+01	1.189E+03	2.599E+01	1.415E+01	8.501E+01	7.557E+01	5.557E+01
F26	Mean	**4.653E+03**	6.015E+03	5.899E+03	4.823E+03	5.736E+03	7.606E+03	6.552E+03	6.583E+03	9.547E+03	7.002E+03	5.396E+03	9.043E+03	1.054E+04	8.500E+03
	Std	**2.479E+02**	5.757E+02	4.344E+02	7.691E+02	1.361E+03	1.709E+02	4.559E+02	5.606E+02	1.511E+03	1.137E+03	3.135E+03	1.983E+03	2.250E+03	1.107E+03
F27	Mean	3.253E+03	3.446E+03	3.398E+03	3.311E+03	3.707E+03	3.449E+03	3.595E+03	3.486E+03	3.747E+03	3.581E+03	3.811E+03	3.723E+03	4.582E+03	**3.200E+03**
	Std	2.373E+01	6.817E+01	6.194E+01	3.943E+01	2.010E+02	2.688E+01	9.863E+01	6.743E+01	1.760E+02	1.280E+02	1.777E+02	1.941E+02	4.882E+02	**4.109E-04**
F28	Mean	**3.274E+03**	4.616E+03	3.302E+03	3.297E+03	3.733E+03	3.358E+03	4.224E+03	3.319E+03	5.265E+03	3.389E+03	3.356E+03	4.127E+03	3.886E+03	3.299E+03
	Std	**2.166E+01**	1.584E+03	2.079E+01	2.226E+01	3.730E+02	2.368E+01	5.035E+02	1.918E+01	2.129E+03	3.479E+01	3.341E+01	1.085E+03	2.002E+02	2.721E+00
F29	Mean	3.813E+03	4.835E+03	4.209E+03	**3.793E+03**	4.424E+03	4.997E+03	4.466E+03	4.537E+03	5.707E+03	4.718E+03	5.095E+03	5.233E+03	6.672E+03	4.985E+03
	Std	2.874E+02	3.556E+02	2.698E+02	**1.959E+02**	3.846E+02	2.531E+02	3.291E+02	3.972E+02	5.369E+02	3.781E+02	4.139E+02	4.946E+02	7.426E+02	3.922E+02
F30	Mean	**8.275E+05**	6.612E+06	8.510E+05	8.392E+05	1.610E+07	1.024E+07	1.162E+08	1.567E+06	2.543E+07	1.429E+06	7.573E+07	5.951E+06	8.940E+07	6.126E+07
	Std	**1.525E+05**	5.218E+06	6.999E+04	1.132E+05	5.821E+07	2.653E+06	4.816E+07	4.467E+05	1.950E+07	5.811E+05	7.104E+06	3.624E+06	3.689E+07	2.476E+07
Average rank		**1.862**	7.310	3.552	2.862	7.793	9.586	9.379	7.655	12.345	6.483	6.621	9.966	12.241	7.345

Note: F2 was omitted. Bold values indicate the best mean for each function. The last row reports the average Friedman rank (lower is better).

Table 8. Statistical results of HPKO and competing algorithms on CEC2017 (100D).

Function	Statistic	**HPKO**	PKO	EPKO	DOA	PSO	DE	GWO	SA	DBO	KEO	TJO	ECO	TTHHO	BWOG
F1	Mean	**1.515E+04**	6.082E+09	9.576E+04	3.710E+06	2.214E+10	2.395E+08	4.137E+10	1.126E+06	6.313E+10	3.363E+07	9.709E+05	2.475E+10	9.503E+09	5.814E+08
	Std	**1.309E+04**	7.031E+09	3.807E+04	8.616E+05	7.363E+09	1.695E+08	8.931E+09	2.225E+06	6.835E+10	1.132E+07	2.241E+05	7.762E+09	1.771E+09	1.692E+08
F3	Mean	2.283E+05	8.109E+05	**7.779E+04**	5.588E+05	5.109E+05	7.758E+05	3.530E+05	1.024E+06	6.483E+05	2.782E+05	2.072E+05	3.202E+05	3.050E+05	2.891E+05
	Std	2.739E+04	1.474E+05	**1.194E+04**	6.697E+04	9.226E+04	5.821E+04	4.725E+04	1.462E+05	3.278E+05	3.604E+04	1.930E+04	8.005E+04	2.110E+04	1.834E+04
F4	Mean	**6.979E+02**	1.593E+03	7.208E+02	7.192E+02	2.926E+03	1.021E+03	4.429E+03	7.132E+02	6.324E+03	9.377E+02	8.306E+02	2.949E+03	2.841E+03	1.146E+03
	Std	**4.257E+01**	5.669E+02	4.988E+01	2.840E+01	1.768E+03	6.652E+01	1.612E+03	5.232E+01	7.298E+03	7.310E+01	4.499E+01	9.313E+02	5.840E+02	6.421E+01
F5	Mean	**7.105E+02**	1.318E+03	1.255E+03	8.934E+02	1.067E+03	1.574E+03	1.159E+03	1.188E+03	1.713E+03	1.184E+03	1.166E+03	1.400E+03	1.614E+03	1.008E+03
	Std	**5.130E+01**	1.132E+02	1.019E+02	4.432E+01	1.012E+02	2.472E+01	7.516E+01	8.893E+01	2.163E+02	6.141E+01	8.877E+01	7.048E+01	6.268E+01	4.701E+01
F6	Mean	6.008E+02	6.389E+02	6.352E+02	6.023E+02	6.305E+02	6.069E+02	6.368E+02	**6.005E+02**	6.773E+02	6.525E+02	6.544E+02	6.697E+02	6.888E+02	6.284E+02
	Std	6.478E-01	2.245E+01	1.023E+01	5.466E-01	6.820E+00	5.795E-01	4.239E+00	**2.044E-01**	1.035E+01	5.362E+00	6.525E+00	4.713E+00	4.381E+00	5.180E+00
F7	Mean	**1.093E+03**	1.972E+03	1.877E+03	1.346E+03	1.774E+03	1.953E+03	2.013E+03	1.723E+03	2.607E+03	2.441E+03	1.743E+03	3.036E+03	3.734E+03	1.520E+03
	Std	**7.940E+01**	3.120E+02	1.166E+02	6.834E+01	1.880E+02	2.889E+01	1.246E+02	1.440E+02	4.343E+02	3.247E+02	1.183E+02	1.945E+02	1.101E+02	9.027E+01
F8	Mean	**1.016E+03**	1.575E+03	1.529E+03	1.191E+03	1.393E+03	1.858E+03	1.482E+03	1.497E+03	2.076E+03	1.523E+03	1.501E+03	1.817E+03	2.059E+03	1.319E+03
	Std	**4.833E+01**	1.555E+02	8.116E+01	4.740E+01	1.461E+02	3.268E+01	1.110E+02	1.047E+02	2.193E+02	7.913E+01	8.801E+01	1.051E+02	6.948E+01	5.828E+01
F9	Mean	**1.459E+03**	2.582E+04	2.771E+04	2.203E+04	3.874E+04	3.696E+04	3.226E+04	5.244E+04	5.467E+04	1.914E+04	2.187E+04	3.507E+04	6.366E+04	1.658E+04
	Std	**9.051E+02**	1.446E+04	3.991E+03	4.637E+03	1.644E+04	5.373E+03	1.250E+04	1.140E+04	2.108E+04	2.615E+03	2.613E+03	3.742E+03	6.683E+03	2.918E+03
F10	Mean	1.575E+04	2.081E+04	2.181E+04	**1.304E+04**	1.910E+04	3.141E+04	1.824E+04	1.509E+04	2.111E+04	1.645E+04	1.638E+04	2.011E+04	2.378E+04	1.535E+04
	Std	1.433E+03	1.551E+03	2.434E+03	**8.600E+02**	3.866E+03	5.291E+02	5.544E+03	1.152E+03	4.825E+03	1.620E+03	1.677E+03	2.207E+03	2.477E+03	1.408E+03
F11	Mean	**2.572E+03**	1.346E+05	2.663E+03	8.270E+03	2.766E+04	1.655E+05	6.124E+04	1.211E+05	1.416E+05	7.280E+03	4.055E+03	5.012E+04	8.143E+04	4.501E+04
	Std	**2.422E+02**	4.485E+04	2.293E+02	3.494E+03	1.681E+04	2.952E+04	1.698E+04	3.934E+04	4.674E+04	2.289E+03	3.101E+02	1.653E+04	2.652E+04	6.926E+03
F12	Mean	**8.441E+06**	6.658E+08	9.388E+06	6.780E+07	7.441E+09	2.520E+09	7.750E+09	6.876E+07	2.610E+09	9.943E+07	3.350E+08	1.741E+09	1.576E+09	4.908E+08
	Std	**4.855E+06**	3.315E+08	3.867E+06	2.848E+07	4.703E+09	4.430E+08	3.733E+09	3.655E+07	1.179E+09	4.244E+07	6.908E+07	1.016E+09	3.497E+08	1.231E+08
F13	Mean	5.460E+03	1.421E+06	**4.715E+03**	8.879E+03	6.282E+08	3.001E+05	8.342E+08	1.338E+05	9.438E+07	3.102E+04	3.331E+04	2.433E+07	2.106E+07	2.748E+07
	Std	4.178E+03	1.577E+06	**2.303E+03**	4.854E+03	6.820E+08	6.700E+05	9.394E+08	2.483E+05	1.135E+08	7.629E+03	7.160E+03	8.738E+07	4.000E+06	1.404E+07
F14	Mean	3.233E+05	6.854E+06	**4.813E+04**	2.853E+06	3.415E+06	2.931E+07	6.178E+06	4.588E+06	9.888E+06	8.720E+05	1.052E+06	4.211E+06	5.762E+06	5.662E+06

Continued on next page

Function	Statistic	**HPKO**	PKO	EPKO	DOA	PSO	DE	GWO	SA	DBO	KEO	TJO	ECO	TTHHO	BWOG
	Std	2.222E+05	3.392E+06	**2.449E+04**	1.392E+06	2.592E+06	9.091E+06	3.291E+06	1.820E+06	8.675E+06	4.268E+05	2.400E+05	2.338E+06	2.290E+06	1.550E+06
F15	Mean	3.913E+03	3.864E+05	**2.416E+03**	4.528E+03	3.005E+08	1.126E+06	1.955E+08	7.924E+04	3.528E+07	1.583E+04	2.669E+04	1.422E+06	5.258E+06	6.330E+06
	Std	2.601E+03	9.832E+05	**7.582E+02**	2.490E+03	5.629E+08	8.768E+05	2.735E+08	1.130E+05	1.035E+08	9.044E+03	7.591E+03	5.060E+06	1.409E+06	1.002E+07
F16	Mean	**4.937E+03**	6.458E+03	5.811E+03	5.180E+03	6.062E+03	1.080E+04	6.195E+03	6.236E+03	8.396E+03	5.841E+03	6.717E+03	7.286E+03	9.109E+03	5.893E+03
	Std	**6.582E+02**	7.278E+02	7.507E+02	4.597E+02	8.626E+02	3.434E+02	7.520E+02	5.907E+02	1.036E+03	8.086E+02	7.302E+02	7.169E+02	1.144E+03	5.140E+02
F17	Mean	4.234E+03	5.527E+03	4.891E+03	**4.097E+03**	5.804E+03	7.477E+03	5.050E+03	5.483E+03	8.340E+03	5.382E+03	5.374E+03	6.307E+03	7.019E+03	4.879E+03
	Std	4.844E+02	6.156E+02	4.826E+02	**3.660E+02**	6.140E+02	2.582E+02	6.257E+02	6.904E+02	9.912E+02	6.241E+02	5.249E+02	7.234E+02	7.224E+02	4.031E+02
F18	Mean	8.542E+05	1.173E+07	**1.412E+05**	3.569E+06	9.348E+06	6.133E+07	6.953E+06	8.204E+06	1.521E+07	1.281E+06	1.624E+06	5.986E+06	6.678E+06	3.566E+06
	Std	4.174E+05	4.827E+06	**3.322E+04**	1.444E+06	1.071E+07	1.405E+07	5.917E+06	5.584E+06	1.119E+07	5.569E+05	5.811E+05	2.916E+06	2.768E+06	9.252E+05
F19	Mean	6.764E+03	4.253E+05	4.107E+03	**4.038E+03**	2.440E+08	1.865E+06	2.278E+08	3.222E+04	4.089E+07	1.931E+04	3.627E+06	3.119E+06	1.667E+07	5.018E+06
	Std	7.041E+03	7.079E+05	2.227E+03	**1.809E+03**	4.264E+08	1.806E+06	2.802E+08	3.208E+04	4.705E+07	2.985E+04	2.220E+06	5.935E+06	1.002E+07	6.297E+06
F20	Mean	4.894E+03	5.245E+03	4.898E+03	**4.338E+03**	5.194E+03	7.189E+03	4.983E+03	5.346E+03	6.401E+03	5.264E+03	5.187E+03	5.611E+03	5.902E+03	4.555E+03
	Std	4.438E+02	5.229E+02	5.357E+02	**3.688E+02**	5.734E+02	2.994E+02	7.980E+02	5.940E+02	7.715E+02	5.231E+02	4.657E+02	4.667E+02	4.799E+02	4.688E+02
F21	Mean	**2.556E+03**	3.019E+03	3.000E+03	2.727E+03	3.093E+03	3.410E+03	2.977E+03	3.046E+03	3.855E+03	2.986E+03	2.883E+03	3.513E+03	4.239E+03	2.894E+03
	Std	**5.644E+01**	1.607E+02	8.787E+01	4.163E+01	1.248E+02	2.698E+01	8.518E+01	1.145E+02	1.707E+02	8.040E+01	6.604E+01	1.811E+02	2.507E+02	5.969E+01
F22	Mean	1.853E+04	2.262E+04	2.465E+04	**1.534E+04**	2.122E+04	3.330E+04	2.118E+04	1.734E+04	2.342E+04	1.887E+04	1.908E+04	2.417E+04	2.686E+04	1.876E+04
	Std	2.258E+03	1.983E+03	1.485E+03	**6.521E+02**	2.523E+03	5.086E+02	4.618E+03	1.274E+03	4.505E+03	1.517E+03	3.495E+03	2.218E+03	2.130E+03	1.186E+03
F23	Mean	3.092E+03	3.478E+03	3.473E+03	**3.086E+03**	4.401E+03	3.734E+03	3.594E+03	3.185E+03	4.362E+03	3.491E+03	3.649E+03	4.176E+03	5.604E+03	3.387E+03
	Std	7.427E+01	1.344E+02	1.097E+02	**4.044E+01**	2.851E+02	2.773E+01	9.806E+01	5.650E+01	2.099E+02	1.083E+02	1.161E+02	1.819E+02	3.578E+02	6.627E+01
F24	Mean	**3.542E+03**	4.077E+03	4.072E+03	3.636E+03	5.585E+03	4.259E+03	4.147E+03	3.895E+03	5.451E+03	4.175E+03	4.154E+03	4.945E+03	7.787E+03	4.097E+03
	Std	**6.281E+01**	1.846E+02	1.036E+02	4.504E+01	5.137E+02	2.916E+01	1.307E+02	9.233E+01	3.444E+02	1.659E+02	1.234E+02	3.171E+02	7.006E+02	1.338E+02
F25	Mean	**3.368E+03**	4.352E+03	3.403E+03	3.386E+03	3.970E+03	4.310E+03	6.006E+03	3.405E+03	8.985E+03	3.625E+03	3.544E+03	5.320E+03	4.687E+03	3.691E+03
	Std	**4.951E+01**	5.592E+02	5.299E+01	3.891E+01	3.118E+02	9.518E+01	7.663E+02	7.837E+01	6.561E+03	7.487E+01	3.834E+01	5.411E+02	2.533E+02	7.228E+01
F26	Mean	**8.260E+03**	1.343E+04	1.409E+04	9.846E+03	1.649E+04	1.627E+04	1.498E+04	1.274E+04	2.524E+04	1.594E+04	2.063E+04	2.453E+04	2.840E+04	1.881E+04
	Std	**6.382E+02**	1.788E+03	1.272E+03	5.324E+02	3.755E+03	2.663E+02	1.285E+03	1.017E+03	3.603E+03	1.705E+03	4.836E+03	3.688E+03	2.003E+03	2.281E+03
F27	Mean	3.405E+03	3.597E+03	3.555E+03	3.485E+03	4.180E+03	4.083E+03	4.062E+03	3.525E+03	4.156E+03	3.840E+03	4.400E+03	4.094E+03	5.784E+03	**3.200E+03**
	Std	2.963E+01	9.198E+01	8.252E+01	3.782E+01	3.471E+02	1.035E+02	1.480E+02	5.670E+01	2.176E+02	1.403E+02	2.098E+02	1.984E+02	9.210E+02	**3.697E-04**

Continued on next page

Function	Statistic	**HPKO**	PKO	EPKO	DOA	PSO	DE	GWO	SA	DBO	KEO	TJO	ECO	TTHHO	BWOG
F28	Mean	3.466E+03	7.127E+03	3.463E+03	3.491E+03	5.657E+03	5.152E+03	8.133E+03	5.693E+03	1.670E+04	3.863E+03	3.604E+03	6.880E+03	5.796E+03	**3.300E+03**
	Std	2.941E+01	4.113E+03	3.984E+01	3.734E+01	1.677E+03	6.376E+02	1.001E+03	4.573E+03	7.398E+03	1.168E+02	4.482E+01	2.919E+03	4.428E+02	**3.382E-04**
F29	Mean	6.027E+03	8.506E+03	7.788E+03	**5.996E+03**	7.240E+03	9.481E+03	8.332E+03	6.922E+03	1.052E+04	7.827E+03	9.564E+03	9.049E+03	1.203E+04	8.307E+03
	Std	6.357E+02	8.997E+02	5.415E+02	**3.774E+02**	6.832E+02	2.852E+02	6.542E+02	5.899E+02	1.707E+03	4.662E+02	8.008E+02	7.468E+02	1.209E+03	4.150E+02
F30	Mean	**1.055E+04**	7.257E+06	1.105E+04	1.517E+05	1.070E+09	2.397E+06	6.564E+08	3.316E+04	9.668E+07	1.264E+06	6.536E+07	6.338E+07	2.155E+08	7.301E+07
	Std	**2.586E+03**	6.696E+06	2.701E+03	1.797E+05	9.463E+08	9.368E+05	4.689E+08	1.495E+04	8.389E+07	4.827E+05	2.030E+07	1.784E+08	9.719E+07	3.837E+07
Average rank		**1.759**	8.690	4.448	2.931	9.276	10.241	9.138	5.931	12.586	5.931	6.448	10.207	11.759	5.655

Note: F2 was omitted. Bold values indicate the best mean for each function. The last row reports the average Friedman rank (lower is better).

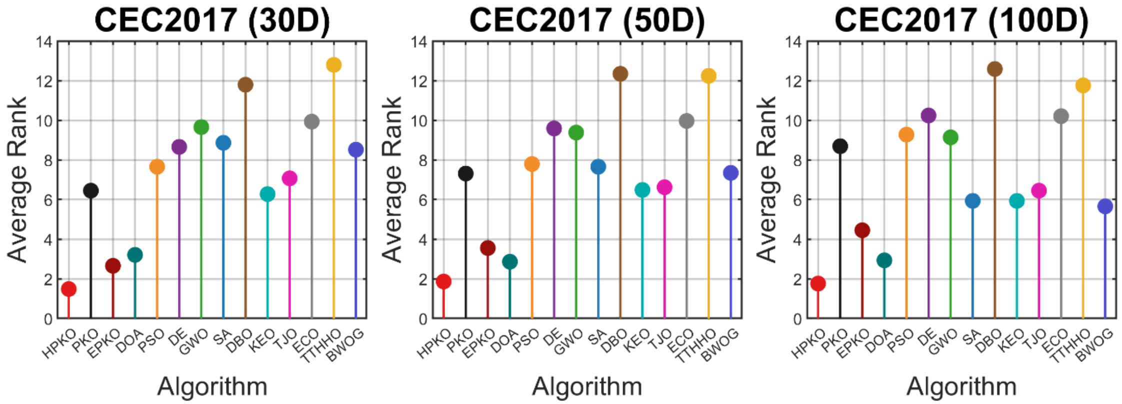

Figure 3. Average Friedman rankings of the compared algorithms on CEC2017 at 30D, 50D, and 100D.

Figure 3 summarizes the average Friedman ranks of the 14 algorithms on CEC2017. HPKO ranks first at 30D, 50D, and 100D. The Friedman tests indicate statistically significant overall differences among the algorithms in all three settings (all $p < 0.001$). The corresponding Holm-adjusted pairwise comparisons and effect sizes are reported in Table 9.

Table 9. Wilcoxon rank-sum results of HPKO against the competing algorithms on CEC2017.

Comparator	30D W/T/L	50D W/T/L	100D W/T/L	Median Cliff's δ (30D/50D/100D)
PKO	28/1/0	29/0/0	29/0/0	+0.940/+0.980/+1.000
EPKO	20/5/4	18/6/5	16/10/3	+0.664/+0.687/+0.664
DOA	22/5/2	19/7/3	17/9/3	+0.602/+0.656/+0.900
PSO	27/2/0	25/4/0	29/0/0	+0.964/+0.991/+1.000
DE	29/0/0	29/0/0	29/0/0	+1.000/+1.000/+1.000
GWO	28/1/0	26/3/0	28/1/0	+1.000/+1.000/+1.000
SA	28/1/0	26/2/1	24/4/1	+0.993/+0.956/+0.962
DBO	29/0/0	29/0/0	29/0/0	+1.000/+1.000/+1.000
KEO	27/2/0	28/1/0	27/2/0	+0.951/+0.956/+1.000
TJO	28/0/1	25/3/1	26/2/1	+0.996/+1.000/+1.000
ECO	29/0/0	29/0/0	29/0/0	+1.000/+1.000/+1.000
TTHHO	29/0/0	29/0/0	29/0/0	+1.000/+1.000/+1.000
BWOG	27/1/1	24/4/1	24/2/3	+1.000/+1.000/+1.000

Note: W/T/L denotes the number of functions on which HPKO is significantly better, not significantly different, or significantly worse at $\alpha=0.05$ after Holm correction. Median Cliff's δ is calculated across functions; positive values favor HPKO.

Table 9 reports the Holm-adjusted pairwise comparisons and Cliff's δ effect sizes. HPKO records more wins than losses against EPKO and DOA at all three dimensions, while the comparisons with the remaining algorithms generally yield larger win counts. The positive median Cliff's δ values further support the overall advantage of HPKO.

Figure 4 presents the mean best-so-far curves for F4, F10, F20 and F30 at 30D, 50D, and 100D. HPKO reaches low objective values rapidly for F4 and F30, while continuing to improve over a longer portion of the search on F10 and F20. Across the selected functions and dimensions, its curves generally remain among the leading trajectories. These curves are consistent with the function-wise results in Tables 6–8 and provide an empirical view of the competitive convergence behavior of HPKO under the tested settings.

Overall, HPKO obtains the lowest average Friedman rank on CEC2017 at 30D, 50D, and 100D. Its leading suite-level rankings, favorable pairwise comparisons, and competitive convergence profiles jointly demonstrate strong and consistent performance across the tested functions and dimensional settings.

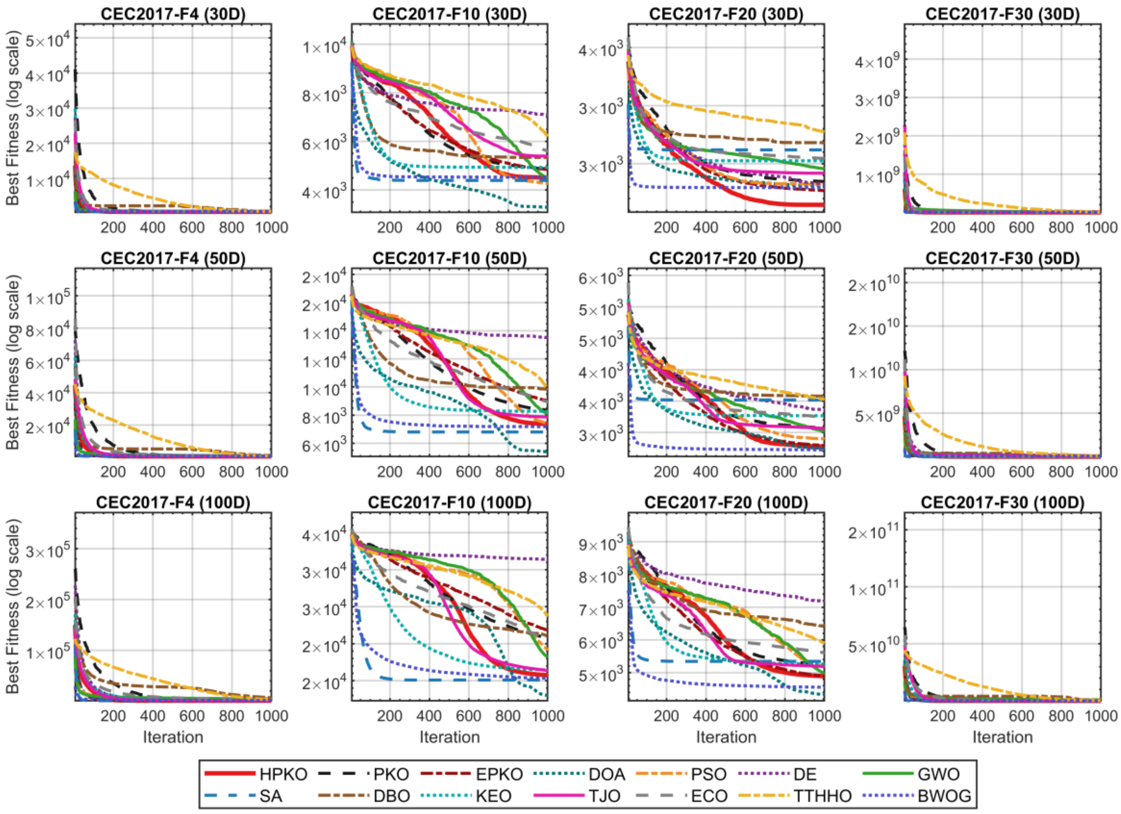

Figure 4. Mean convergence curves of representative CEC2017 functions at 30D, 50D, and 100D.

4.3.2. Results on the CEC2022 benchmark suite

Comparative tests were also conducted on the CEC2022 benchmark suite at 10D and 20D to evaluate HPKO on a second benchmark family.

Table 10 presents the CEC2022 results at 10D. HPKO obtains the lowest average Friedman rank of 2.167, followed by EPKO, PKO, and DOA with ranks of 3.917, 4.833, and 5.167, respectively. At the function level, HPKO achieves the lowest or tied-lowest mean values on seven of the 12 functions, including the lowest mean values on all three hybrid functions, F6–F8. These results place HPKO in the leading overall position on the 10-dimensional suite.

With the dimension increased to 20, HPKO remains the top-ranked algorithm in Table 11, achieving an average Friedman rank of 1.833, compared with 2.917 for EPKO and 4.500 for DOA. Its leading position is also reflected in the function-wise results, where it obtains the lowest or tied-lowest mean values on 8 of the 12 functions, including 2 hybrid functions and 3 composition functions. The breadth of these favorable results demonstrates the strong overall competitiveness of HPKO on the 20-dimensional CEC2022 suite.

Table 10. Statistical results of HPKO and competing algorithms on CEC2022 (10D).

Function	Statistic	**HPKO**	PKO	EPKO	DOA	PSO	DE	GWO	SA	DBO	KEO	TJO	ECO	TTHHO	BWOG
F1	Mean	**3.000E+02**	3.450E+02	**3.000E+02**	**3.000E+02**	**3.000E+02**	1.939E+03	1.553E+03	4.037E+03	3.501E+02	**3.000E+02**	**3.000E+02**	3.002E+02	3.154E+02	1.237E+03
	Std	**0.000E+00**	9.505E+01	**0.000E+00**	**3.261E-04**	**2.523E-08**	5.781E+02	1.983E+03	3.512E+03	1.154E+02	**2.793E-14**	**1.884E-05**	3.051E-01	3.522E+01	8.759E+02
F2	Mean	4.041E+02	4.066E+02	4.044E+02	4.024E+02	4.187E+02	4.081E+02	4.225E+02	4.146E+02	4.155E+02	4.077E+02	**4.013E+02**	4.150E+02	4.285E+02	4.444E+02
	Std	3.200E+00	1.941E+00	3.425E+00	3.193E+00	2.229E+01	6.990E-01	2.224E+01	2.199E+01	2.121E+01	1.178E+01	**2.768E+00**	2.419E+01	2.822E+01	2.250E+01
F3	Mean	**6.000E+02**	**6.000E+02**	**6.000E+02**	**6.000E+02**	6.002E+02	**6.000E+02**	6.007E+02	**6.000E+02**	6.039E+02	6.002E+02	6.019E+02	6.112E+02	6.373E+02	6.052E+02
	Std	**0.000E+00**	**5.374E-02**	**1.034E-13**	**1.036E-03**	8.117E-01	**8.444E-14**	9.527E-01	**2.981E-03**	5.703E+00	5.006E-01	1.360E+00	1.002E+01	9.762E+00	2.566E+00
F4	Mean	8.088E+02	8.124E+02	**8.058E+02**	8.153E+02	8.100E+02	8.191E+02	8.139E+02	8.445E+02	8.306E+02	8.184E+02	8.117E+02	8.233E+02	8.261E+02	8.096E+02
	Std	3.911E+00	5.838E+00	**2.433E+00**	5.827E+00	4.324E+00	3.589E+00	6.510E+00	2.098E+01	1.279E+01	9.741E+00	5.051E+00	7.038E+00	8.804E+00	3.449E+00
F5	Mean	**9.000E+02**	**9.000E+02**	**9.000E+02**	9.052E+02	9.001E+02	**9.000E+02**	9.100E+02	1.757E+03	9.288E+02	9.099E+02	**9.000E+02**	1.044E+03	1.326E+03	9.171E+02
	Std	**0.000E+00**	**6.936E-03**	**1.635E-02**	5.988E+00	2.357E-01	**1.683E-07**	1.941E+01	5.727E+02	5.220E+01	2.232E+01	**1.018E-01**	1.537E+02	1.356E+02	1.348E+01
F6	Mean	**1.800E+03**	3.853E+03	1.815E+03	2.233E+03	6.039E+03	4.374E+03	6.712E+03	5.446E+03	5.269E+03	1.860E+03	2.481E+03	4.775E+03	4.973E+03	2.213E+03
	Std	**3.249E-01**	1.462E+03	1.491E+01	6.245E+02	2.556E+03	1.560E+03	2.413E+03	2.183E+03	2.288E+03	5.788E+01	8.034E+02	2.391E+03	3.434E+03	5.383E+02
F7	Mean	**2.002E+03**	2.016E+03	2.019E+03	2.005E+03	2.017E+03	2.003E+03	2.029E+03	2.019E+03	2.024E+03	2.024E+03	2.029E+03	2.032E+03	2.068E+03	2.033E+03
	Std	**3.906E+00**	8.185E+00	5.126E+00	8.378E+00	8.616E+00	2.272E+00	2.208E+01	4.993E+00	6.676E+00	7.991E+00	6.451E+00	1.642E+01	3.040E+01	9.631E+00
F8	Mean	**2.207E+03**	2.222E+03	2.218E+03	2.211E+03	2.223E+03	2.216E+03	2.224E+03	2.220E+03	2.227E+03	2.220E+03	2.220E+03	2.224E+03	2.232E+03	2.224E+03
	Std	**9.142E+00**	9.389E-01	6.897E+00	9.032E+00	2.304E+01	5.171E+00	4.795E+00	3.526E+00	7.481E+00	3.827E+00	7.152E+00	5.668E+00	1.263E+01	2.102E+00
F9	Mean	**2.529E+03**	**2.529E+03**	**2.529E+03**	**2.529E+03**	2.542E+03	**2.529E+03**	2.556E+03	2.532E+03	2.539E+03	**2.529E+03**	**2.529E+03**	2.539E+03	2.590E+03	2.593E+03
	Std	**0.000E+00**	**8.770E-09**	**0.000E+00**	**3.924E-05**	3.450E+01	**0.000E+00**	3.710E+01	5.536E+00	3.506E+01	**1.194E-13**	**3.143E-02**	3.728E+01	4.043E+01	3.417E+01
F10	Mean	2.500E+03	2.500E+03	2.500E+03	**2.421E+03**	2.566E+03	2.501E+03	2.569E+03	2.486E+03	2.546E+03	2.526E+03	2.504E+03	2.569E+03	2.577E+03	2.516E+03
	Std	2.901E-02	6.782E-02	6.529E-02	**4.055E+01**	5.808E+01	2.044E-01	7.920E+01	9.117E+01	6.528E+01	5.187E+01	2.161E+01	6.384E+01	6.820E+01	3.834E+01
F11	Mean	2.700E+03	**2.640E+03**	2.900E+03	2.846E+03	2.674E+03	2.893E+03	2.909E+03	2.997E+03	2.794E+03	2.875E+03	2.766E+03	2.719E+03	2.749E+03	2.959E+03
	Std	1.438E+02	**1.037E+02**	3.776E-13	1.007E+02	1.435E+02	2.791E+01	1.170E+02	3.903E+02	1.289E+02	7.973E+01	1.451E+02	1.751E+02	1.272E+02	1.683E+02
F12	Mean	2.863E+03	**2.861E+03**	2.862E+03	2.865E+03	2.875E+03	**2.861E+03**	2.864E+03	2.865E+03	2.866E+03	2.864E+03	2.864E+03	2.867E+03	2.905E+03	2.868E+03
	Std	1.349E+00	**9.849E-01**	1.664E+00	1.674E+00	2.442E+01	**1.204E+00**	2.445E+00	1.824E+00	2.683E+00	1.102E+00	1.720E+00	1.245E+01	3.751E+01	1.411E+00
Average rank		**2.167**	4.833	3.917	5.167	8.083	5.667	10.583	9.083	10.417	6.417	6.167	10.083	12.000	10.417

Note: Bold values indicate the best mean for each function. The last row reports the average Friedman rank (lower is better).

Table 11. Statistical results of HPKO and competing algorithms on CEC2022 (20D).

Function	Statistic	**HPKO**	PKO	EPKO	DOA	PSO	DE	GWO	SA	DBO	KEO	TJO	ECO	TTHHO	BWOG
F1	Mean	**3.000E+02**	1.375E+04	**3.000E+02**	4.565E+02	8.276E+02	2.785E+04	9.687E+03	3.004E+04	1.390E+04	3.045E+02	**3.000E+02**	4.241E+03	9.739E+03	1.311E+04
	Std	**3.049E-08**	5.560E+03	**6.064E-14**	1.936E+02	4.558E+02	5.651E+03	4.333E+03	1.415E+04	8.378E+03	5.961E+00	**3.247E-03**	2.845E+03	4.251E+03	3.412E+03
F2	Mean	4.478E+02	4.498E+02	4.427E+02	**4.416E+02**	4.636E+02	4.491E+02	4.995E+02	4.446E+02	4.864E+02	4.519E+02	4.537E+02	4.644E+02	4.972E+02	5.354E+02
	Std	1.952E+00	6.955E+00	1.663E+01	**1.763E+01**	2.091E+01	7.064E-03	3.925E+01	1.502E+01	5.818E+01	1.365E+01	9.416E+00	2.422E+01	3.952E+01	4.513E+01
F3	Mean	**6.000E+02**	6.007E+02	**6.000E+02**	**6.000E+02**	6.015E+02	**6.000E+02**	6.045E+02	**6.000E+02**	6.191E+02	6.064E+02	6.129E+02	6.340E+02	6.586E+02	6.118E+02
	Std	**8.540E-06**	7.994E-01	**1.610E-02**	**5.657E-03**	2.189E+00	**1.552E-07**	3.621E+00	**3.411E-03**	9.159E+00	5.539E+00	5.792E+00	1.160E+01	8.454E+00	4.441E+00
F4	Mean	8.321E+02	8.371E+02	**8.262E+02**	8.502E+02	8.324E+02	9.046E+02	8.502E+02	9.062E+02	9.104E+02	8.453E+02	8.543E+02	8.728E+02	8.879E+02	8.481E+02
	Std	1.064E+01	1.264E+01	**5.263E+00**	1.477E+01	1.548E+01	8.793E+00	2.337E+01	2.822E+01	2.663E+01	1.611E+01	1.510E+01	1.913E+01	1.146E+01	9.430E+00
F5	Mean	**9.000E+02**	9.122E+02	9.013E+02	1.263E+03	9.114E+02	9.186E+02	1.115E+03	5.942E+03	1.769E+03	1.086E+03	9.268E+02	2.202E+03	2.765E+03	1.039E+03
	Std	**1.635E-02**	2.339E+01	2.609E+00	3.102E+02	8.460E+00	1.558E+01	2.117E+02	2.047E+03	5.930E+02	1.473E+02	3.921E+01	3.575E+02	2.810E+02	9.038E+01
F6	Mean	**2.145E+03**	2.494E+04	2.767E+03	2.603E+03	1.049E+05	1.564E+06	1.067E+06	1.459E+04	6.640E+04	6.258E+03	2.980E+03	6.622E+03	1.687E+05	1.080E+05
	Std	**7.512E+02**	1.119E+04	1.502E+03	1.099E+03	3.766E+05	7.361E+05	3.571E+06	9.714E+03	2.015E+05	4.338E+03	1.387E+03	7.281E+03	7.495E+04	2.320E+05
F7	Mean	**2.024E+03**	2.051E+03	2.051E+03	2.035E+03	2.044E+03	2.041E+03	2.096E+03	2.117E+03	2.123E+03	2.082E+03	2.084E+03	2.115E+03	2.158E+03	2.077E+03
	Std	**5.017E+00**	1.531E+01	1.355E+01	1.439E+01	2.574E+01	5.445E+00	5.425E+01	6.066E+01	4.546E+01	3.607E+01	2.067E+01	4.721E+01	3.286E+01	1.338E+01
F8	Mean	2.224E+03	2.229E+03	2.226E+03	**2.221E+03**	2.255E+03	2.228E+03	2.250E+03	2.284E+03	2.297E+03	2.231E+03	2.227E+03	2.266E+03	2.246E+03	2.235E+03
	Std	2.417E+00	4.428E+00	1.341E+00	**2.435E+00**	5.319E+01	1.201E+00	4.486E+01	7.306E+01	7.520E+01	2.611E+01	1.508E+00	6.091E+01	2.264E+01	2.999E+01
F9	Mean	**2.481E+03**	**2.481E+03**	**2.481E+03**	**2.481E+03**	2.501E+03	**2.481E+03**	2.508E+03	2.485E+03	2.493E+03	**2.481E+03**	**2.481E+03**	2.482E+03	2.525E+03	2.519E+03
	Std	**3.482E-13**	**2.443E-02**	**3.045E-13**	**2.211E-01**	2.445E+01	**2.201E-05**	2.786E+01	4.192E+00	1.815E+01	**7.013E-07**	**1.852E-01**	1.135E+00	3.518E+01	9.986E+00
F10	Mean	2.504E+03	3.319E+03	2.991E+03	**2.431E+03**	2.972E+03	2.513E+03	3.282E+03	2.436E+03	2.849E+03	3.541E+03	2.693E+03	3.390E+03	3.672E+03	2.570E+03
	Std	2.196E+01	8.690E+02	7.856E+02	**4.781E+01**	3.541E+02	1.982E+01	7.017E+02	4.837E+01	7.154E+02	6.791E+02	5.284E+02	9.478E+02	7.880E+02	1.456E+02
F11	Mean	**2.900E+03**	2.908E+03	**2.900E+03**	2.902E+03	**2.900E+03**	**2.900E+03**	3.528E+03	2.901E+03	2.913E+03	**2.900E+03**	2.901E+03	2.964E+03	3.149E+03	3.356E+03
	Std	**1.218E-12**	7.135E+00	**1.351E-12**	3.451E-01	**2.699E-03**	**5.268E-08**	4.886E+02	3.921E+00	3.462E+01	**4.000E-08**	2.272E-01	1.288E+02	7.537E+02	1.886E+02
F12	Mean	**2.937E+03**	2.942E+03	2.941E+03	2.945E+03	2.999E+03	2.941E+03	2.967E+03	2.959E+03	2.996E+03	2.959E+03	2.976E+03	2.998E+03	3.096E+03	2.980E+03
	Std	**3.610E+00**	1.819E+00	3.762E+00	6.613E+00	4.631E+01	2.000E+00	2.962E+01	1.304E+01	2.663E+01	1.912E+01	2.015E+01	4.562E+01	8.926E+01	1.589E+01
Average rank		**1.833**	6.667	2.917	4.500	7.500	6.083	10.167	8.583	11.167	6.500	6.917	10.333	12.333	9.500

Note: Bold values indicate the best mean for each function. The last row reports the average Friedman rank (lower is better).

Figure 5 further presents the average Friedman rankings of the 14 algorithms on CEC2022 at 10D and 20D. Tables 10 and 11 report the function-wise numerical results, and the Friedman rankings provide an overall rank-based comparison across the complete benchmark suite. HPKO ranks first in both dimensional settings, with average ranks of 2.167 and 1.833, respectively, and the Friedman tests indicate significant overall differences among the algorithms in both cases (all $p < 0.001$). The corresponding Holm-adjusted pairwise comparisons and Cliff's δ effect sizes are reported in Table 12.

Table 12 presents the Holm-adjusted pairwise results for CEC2022. Against EPKO, HPKO records W/T/L counts of 4/7/1 at 10D and 6/4/2 at 20D, with positive median Cliff's δ values of 0.250 and 0.397, respectively. Its advantage over DOA is more pronounced, with corresponding counts of 8/3/1 and 9/0/3 and median effect sizes of 0.751 and 0.729. Against the remaining competitors, HPKO generally records 9–12 wins at 10D and 10–12 wins at 20D, providing further statistical support for its leading positions in the Friedman rankings.

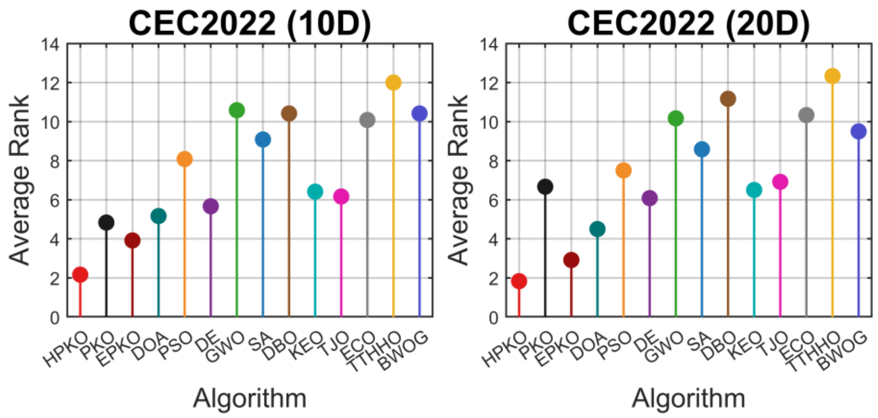

Figure 5. Average Friedman rankings of the compared algorithms on CEC2022 at 10D and 20D.

Table 12. Holm-adjusted pairwise Wilcoxon rank-sum results of HPKO against the competing algorithms on CEC2022.

Comparator	10D W/T/L	20D W/T/L	Median Cliff's δ (10D/20D)
PKO	10/0/2	11/1/0	+0.750/+0.981
EPKO	4/7/1	6/4/2	+0.250/+0.397
DOA	8/3/1	9/0/3	+0.751/+0.729
PSO	10/1/1	11/1/0	+0.759/+0.989
DE	9/2/1	11/1/0	+0.679/+1.000
GWO	12/0/0	12/0/0	+0.967/+0.992
SA	11/1/0	10/0/2	+0.947/+0.986
DBO	11/1/0	12/0/0	+0.918/+1.000
KEO	10/2/0	11/1/0	+0.770/+0.990
TJO	11/1/0	12/0/0	+0.900/+1.000
ECO	12/0/0	12/0/0	+0.964/+0.987
TTHHO	12/0/0	12/0/0	+1.000/+1.000
BWOG	11/1/0	12/0/0	+0.998/+1.000

Note: W/T/L denotes the number of functions on which HPKO is significantly better, not significantly different, or significantly worse at α=0.05 after Holm correction. Median Cliff's δ is calculated across functions; positive values favor HPKO.

Figure 6 shows the mean best-so-far curves for F4, F8, F9, and F12 at 10D and 20D. On F4, HPKO continues to refine the solution through the middle and late stages of the search and finishes among the lowest trajectories in both dimensions. On F8, F9, and F12, it rapidly enters the leading group and retains competitive final objective values after the initial descent. These curves demonstrate the competitive numerical convergence of HPKO across representative multimodal, hybrid, and composition functions under both dimensional settings.

Overall, the CEC2022 analysis places HPKO first at 10D and 20D. Favorable function-wise outcomes, Holm-adjusted comparisons, positive median Cliff's δ values, and competitive convergence curves jointly support its leading suite-level performance. In conjunction with the CEC2017 findings, the benchmark evidence shows that HPKO maintains the top overall position across both CEC suites and all tested dimensional settings.

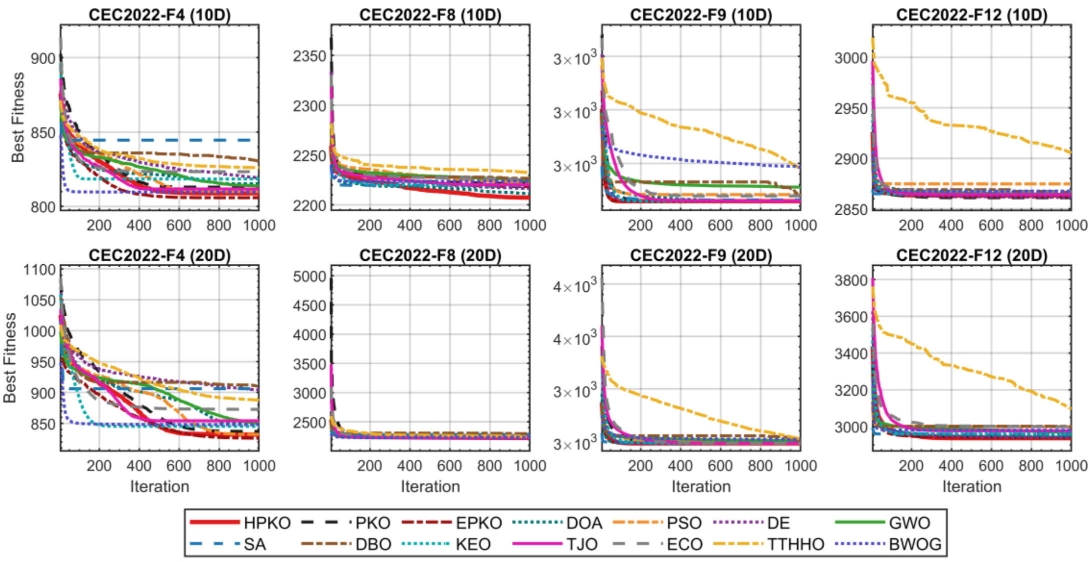

Figure 6. Mean convergence curves of representative CEC2022 functions at 10D and 20D.

5. 3D UAV path planning simulations

After the ablation and benchmark studies on synthetic test functions, in this section, we further examine the applicability of HPKO to 3D UAV path planning in terrain–threat environments. In this application, each candidate solution represents the coordinates of four intermediate waypoints. IBC first confines these coordinates to the prescribed search bounds, after which the fixed start and goal are appended, and the resulting trajectory is evaluated according to the terrain-clearance and threat-avoidance requirements and the composite cost in (18). The trajectory cost is then returned to HPKO as the fitness value. Compared with standard benchmark functions, the two flight scenarios provide an application-oriented test under coupled geometric, safety, and maneuvering constraints. The hills and threat regions create separated or narrow feasible corridors, while the coupled path-length, threat-exposure, altitude, and smoothness terms yield competing route patterns. These characteristics correspond to the intended roles of the three HPKO modules: CTI improves the initial coverage of waypoint configurations, ROBL introduces alternative candidates when stagnation or low population diversity is detected, and IBC repairs coordinate-bound violations while preserving useful update directions.

5.1. Simulation environment and parameter settings

The UAV path-planning task considered in this section is to generate a collision-free three-dimensional trajectory in a known environment, enabling the vehicle to travel from a prescribed start position to a specified target while satisfying safety and mission-related requirements. The simulation environment follows the modeling framework established in Section 2. The terrain is constructed by superimposing a trigonometric base surface and multiple Gaussian hills, while cylindrical threat zones are used to represent radar coverage or no-fly regions.

To evaluate the performance of HPKO under different task difficulties, two simulation scenarios are considered: A simple environment and a complex environment. Both scenarios share the horizontal workspace [0,100] × [0,100]. The simple environment contains four Gaussian hills and three cylindrical threat regions, whereas the complex environment adds three hills and four threat regions to produce narrower feasible corridors and denser threat coverage. The corresponding terrain and threat parameters are listed in Tables 13 and 14.

Table 13. Gaussian hill parameters for the simple and complex environments.

Environment	Hill	x_i	y_i	$\sigma_{x,i}$	$\sigma_{y,i}$	h_i
Simple and complex	1	25	35	6	6	35
	2	65	45	9	9	42
	3	85	75	7	7	38
	4	45	85	5	5	32
Complex only	5	15	80	5	5	30
	6	80	20	6	6	28
	7	55	70	7	7	36

Table 14. Cylindrical threat parameters for the simple and complex environments.

Environment	Threat	x_j	y_j	R_j	h_j
Simple and complex	1	40	25	8	25
	2	75	65	9	30
	3	50	60	10	35
Complex only	4	30	50	7	25
	5	60	20	9	28
	6	70	80	6	30
	7	15	65	8	20

The UAV start and goal positions are set to (5, 5, 20) and (95, 95, 20), respectively. Four intermediate waypoints are introduced in addition to the fixed endpoints, so that each candidate trajectory is represented by six three-dimensional waypoints. For trajectory evaluation, each segment is sampled at 20 evenly spaced points, and the external threat-buffer width in the threat-cost formulation is fixed at 5 m. The default objective weights are $(w_1, w_2, w_3, w_4) = (0.40, 0.30, 0.20, 0.10)$.

This setting is used as a balanced reference that prioritizes route length while retaining explicit contributions from buffered threat exposure, altitude cost, and smoothness; alternative length- and threat-priority settings are examined in Section 5.4. HPKO, PKO, PSO, and GWO use the same waypoint representation, objective function, search bounds, population size of 50, and maximum iteration count of 500, while their algorithm-specific control parameters follow Table 3. All simulations were implemented in MATLAB R2021b on a Windows 11 desktop equipped with an Intel Core i5-8300H CPU at 2.30 GHz and 16 GB of RAM. The random seeds were fixed in advance to support reproducibility.

5.2. Results in the simple environment

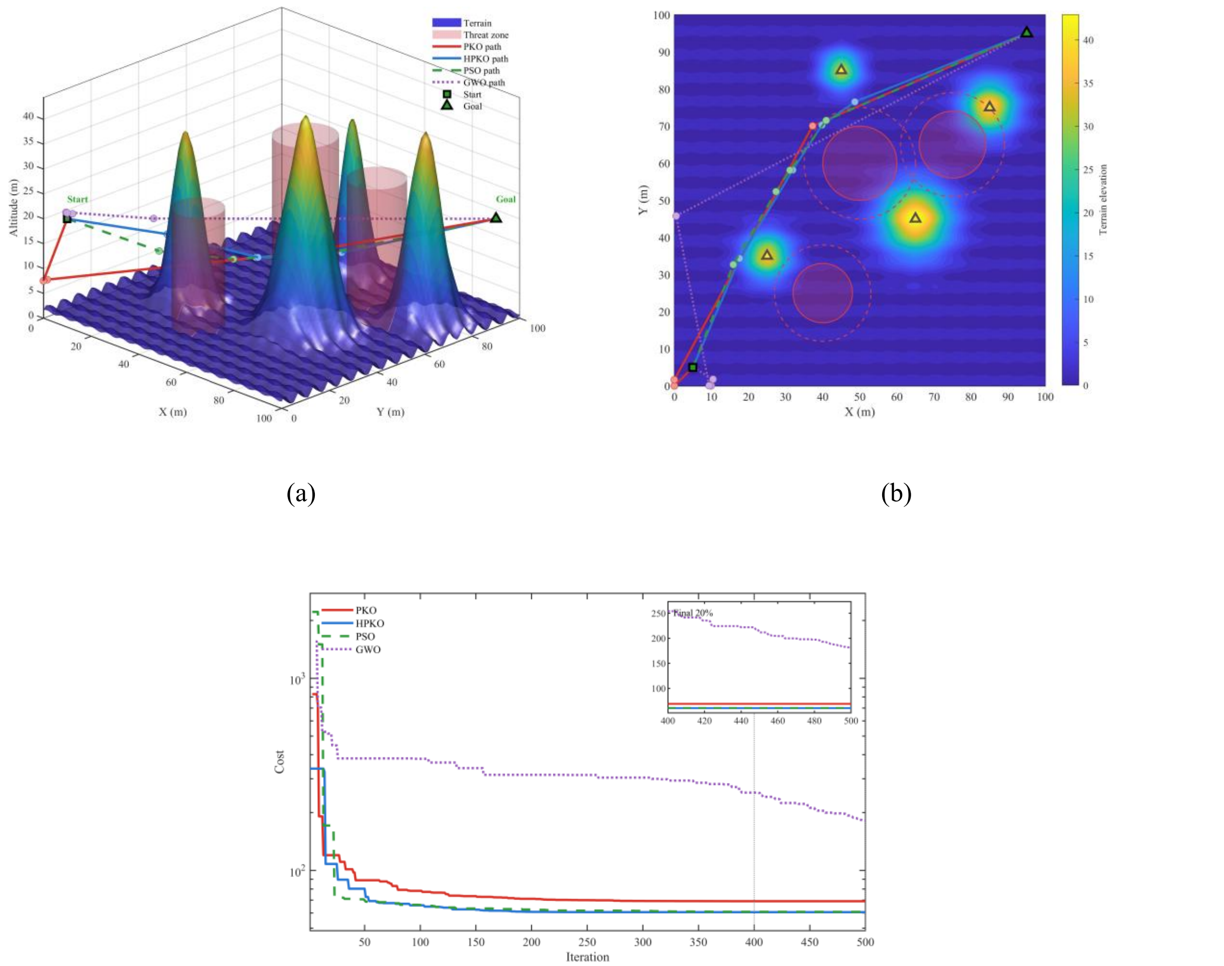

(a) (b) (c)

Figure 7. Simulation results in the simple environment. (a) Three-dimensional view. (b) Top view. (c) Convergence curves.

In the simple environment, all four algorithms generate feasible three-dimensional trajectories connecting the start and goal while satisfying the terrain-clearance and hard threat-exclusion requirements (Figure 7). HPKO, PKO, and PSO use a similar passage between the central obstacles, whereas GWO introduces a pronounced detour near the beginning of the path and produces a less compact route. The trajectories obtained by HPKO and PSO are close in geometry, with composite costs of 60.610 and 60.833, respectively (Table 15). Relative to PKO, HPKO connects the intermediate waypoints more directly and reduces the path-length term by 12.9%, from 158.075 to 137.631. The convergence curves further show that HPKO and PSO enter the low-cost region rapidly, while HPKO attains the lowest final objective value (Figure 7c).

5.3. Results in the complex environment

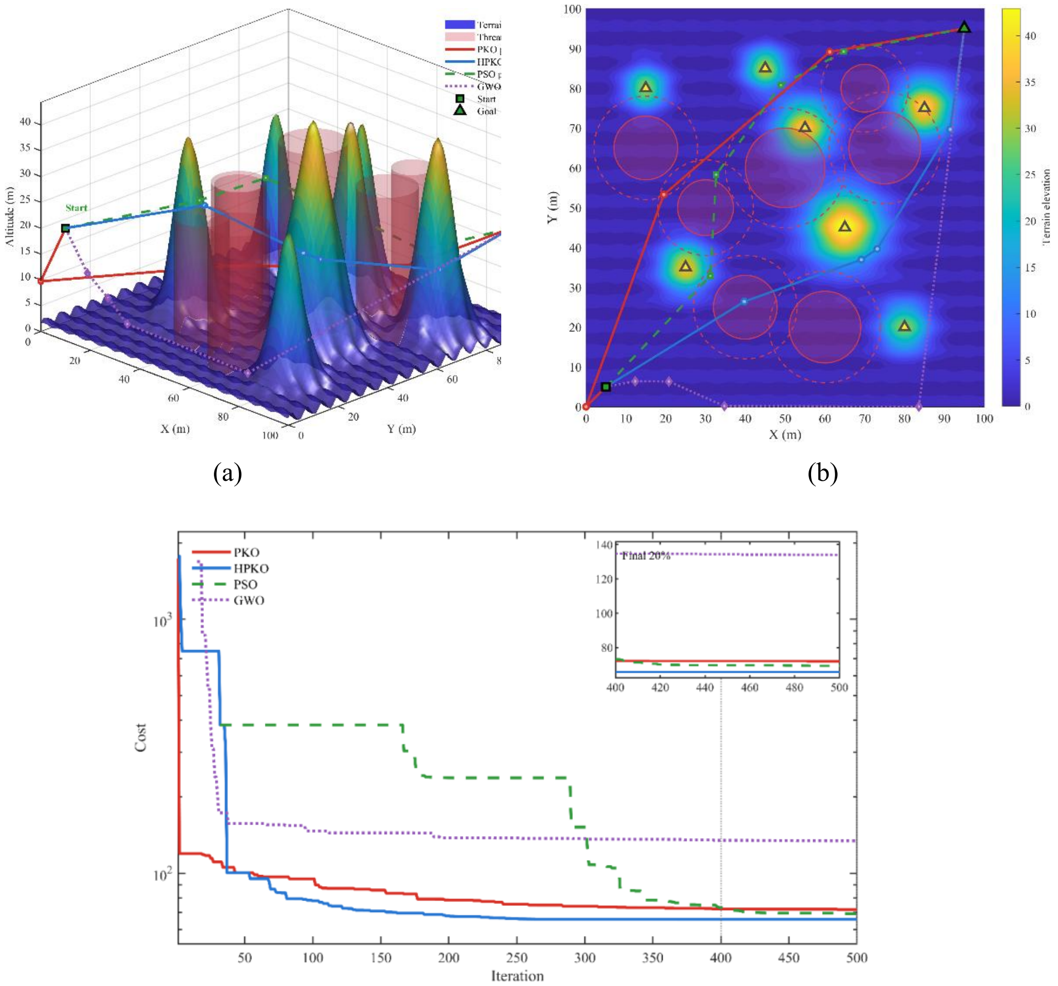

(a) (b)

(c)

Figure 8. Simulation results in the complex environment. (a) Three-dimensional view. (b) Top view. (c) Convergence curves.

The complex environment imposes a higher level of difficulty because the additional hills and threat zones narrow the feasible passages and strengthen the coupling among terrain, threats, and maneuvering constraints. As shown in Figure 8(a),(b), HPKO follows the interior corridors through the dense obstacle region and forms a relatively compact trajectory. PKO adopts a comparable general direction but uses a longer route, whereas GWO moves along the workspace boundary to bypass the central region. PSO produces a slightly shorter path than HPKO but makes considerably larger altitude adjustments. This difference is reflected in Table 15 and explains why its composite cost remains higher.

Overall, HPKO obtains the lowest cost by maintaining a more balanced trajectory across the horizontal and vertical dimensions.

The convergence curves show that all four algorithms achieve substantial cost reductions during the early search stage. HPKO continues to improve after the initial descent and stabilizes at the lowest objective level. PKO and PSO approach similar but higher final values, whereas GWO converges more slowly and remains above the other methods during the later iterations (Figure 8c). The separation is more evident than in the simple environment, indicating that the advantage of HPKO becomes clearer as the feasible corridors narrow and the path constraints become more strongly coupled. The continued improvement after the initial descent and the compact interior-corridor trajectory are consistent with the intended effects of broader initial coverage and state-triggered diversity recovery. In the CEC ablation study, ROBL is the strongest standalone module, while the complete HPKO achieves the best overall rank.

Table 15. Composite and component costs of the four algorithms in the two UAV environments.

Scenario	Algorithm	J	Cost components			
			J_{len}	J_{thr}	J_{alt}	J_{sm}
Simple	HPKO	**60.610**	137.631	0.227	27.450	0.000
	PKO	69.100	158.075	0.102	29.200	0.000
	PSO	60.833	138.119	0.295	27.483	0.000
	GWO	181.552	163.975	9.993	79.670	970.301
Complex	HPKO	**63.526**	143.210	2.509	27.450	0.000
	PKO	72.419	159.968	2.559	38.323	0.000
	PSO	73.321	140.085	0.038	85.917	0.922
	GWO	109.400	185.890	0.000	78.923	192.592

Note: J is evaluated using (w_1, w_2, w_3, w_4) = (0.40, 0.30, 0.20, 0.10). Bold values indicate the lowest composite cost in each environment.

5.4. Weight sensitivity analysis

Table 16 summarizes the sensitivity of the HPKO path-cost components to the three objective-weighting schemes in the complex environment. Variation in the objective weights affects the resulting trajectory geometry rather than merely rescaling the composite objective value. Under the threat-priority configuration, the buffered threat exposure decreases from 2.509 to 1.158, whereas the path-length and altitude-cost terms increase from 143.210 to 144.761 and from 27.450 to 36.828, respectively. By contrast, the length-priority configuration reduces the path length to 141.936 but increases the buffered threat exposure to 4.115 and the altitude cost to 29.601. These changes demonstrate that the objective components are interdependent because each weighting scheme alters the spatial distribution of the optimized waypoints. Relative to the two priority-oriented configurations, the default setting produces intermediate values for path length and threat exposure while retaining the lowest altitude cost. It therefore represents a balanced trade-off among route compactness, threat avoidance, and altitude variation. Moreover, all three weighting schemes yield feasible trajectories without incurring a smoothness penalty.

Table 16. Sensitivity of HPKO path-cost components to the objective weights in the complex environment.

Weighting scheme	Weight coefficients				Cost components			
	w_1	w_2	w_3	w_4	J_{len}	J_{thr}	J_{alt}	J_{sm}
Default	0.40	0.30	0.20	0.10	143.210	2.509	27.450	0
Length-priority	0.55	0.20	0.15	0.10	141.936	4.115	29.601	0
Threat-priority	0.30	0.50	0.15	0.05	144.761	1.158	36.828	0

Overall, HPKO produces feasible trajectories and attains the lowest composite objective value among the four compared algorithms in both test environments. In the simple environment, its performance is comparable to that of PSO, with composite objective values of 60.610 and 60.833, respectively. The advantage of HPKO becomes more pronounced in the complex environment, where its composite objective value is lower than those of PKO, PSO, and GWO. Although PSO generates a slightly shorter path, this reduction is accompanied by a substantially higher altitude cost and a nonzero smoothness penalty. Moreover, HPKO avoids the boundary detour exhibited by GWO and yields a shorter route than PKO. The sensitivity results further indicate that adjustments to the objective weights systematically modify the balance among path length, buffered threat exposure, and altitude-related cost.

6. Conclusions and future work

In this paper, we proposed a hybrid pied kingfisher optimizer (HPKO) for constrained continuous optimization, with three-dimensional UAV path planning considered as a representative application. Built on the original PKO, HPKO integrates Tent chaotic initialization, multi-elite ROBL, and IBC to improve initial search-space coverage, recover population diversity during stagnation, and repair out-of-bound candidates while preserving useful search directions. Under a bounded search domain and a lower-bounded objective function, the convergence analysis establishes that the historical population-best objective sequence converges to a finite limit. In the ablation study, ROBL provides the strongest standalone improvement, whereas the full HPKO obtains an average rank of 1.17 and ranks first on 24 of the 29 CEC2017 functions, with significant differences over PKO and the three single-module variants. Across CEC2017 at 30D, 50D, and 100D and CEC2022 at 10D and 20D, HPKO achieves the lowest average Friedman rank in all five settings. The Holm-adjusted pairwise comparisons and positive median Cliff's δ values further support its leading benchmark performance.

For the engineering application, a three-dimensional UAV path-planning framework was established using a trigonometric base surface, Gaussian hills, and cylindrical threat zones. The trajectory evaluation combines hard terrain-clearance and threat-exclusion requirements with path-length, buffered threat-exposure, altitude, and smoothness costs. In the simple and complex environments, HPKO achieves the lowest composite cost among HPKO, PKO, PSO, and GWO. Its result is close to that of PSO in the simple environment, while the advantage becomes clearer in the complex environment, where the slightly lower path-length cost of PSO is accompanied by a substantially higher altitude cost. The weight sensitivity analysis further shows that changing the objective weights systematically shifts the balance among path length, buffered threat exposure, and altitude cost while preserving trajectory feasibility. These results support the applicability of HPKO to constrained three-dimensional UAV path planning under the tested terrain–threat settings.

This study is limited to synthetic terrain, static threat regions, and offline path planning. Further evaluation is therefore required using real digital elevation maps, sensing uncertainty, time-varying threats, and environmental updates. The comparisons also focus on population-based metaheuristics and do not include learning-based or model-based planners such as deep reinforcement learning and model predictive control. In future work, we will extend HPKO to dynamic path planning and rapid replanning, examine multi-objective formulations for explicitly representing competing mission criteria, and investigate adaptive parameter control. Comparisons with other planning paradigms will provide a broader assessment of its applicability under realistic UAV operating conditions.

Author contributions

Qiaoping Li: Conceptualization, Methodology, Supervision, Funding acquisition, Writing-review and editing. **Jiahao Wan:** Software, Validation, Formal analysis, Investigation, Data curation, Visualization, Writing-original draft. **All authors** have read and agreed to the published version of the manuscript.

Use of Generative-AI tools declaration

The authors used ChatGPT (OpenAI) solely to assist with language refinement and structural editing throughout the manuscript. All scientific content, methodology, data, numerical results, figures, tables, and conclusions were independently reviewed and verified by the authors, who take full responsibility for the final content.

Acknowledgments

This work was supported by the Key Science and Technology Project of Henan Province with Grant Nos. 242102220043, 262102220005 and the Key Research Project of Henan Higher Education Institutions with Grant No. 24A590005. The authors would like to thank the editor and reviewers for their valuable comments.

Conflict of interest

The authors declare no conflicts of interest.

References

1. M. Moshref-Javadi, A. Hemmati, M. Winkenbach, A truck and drones model for last-mile delivery: A mathematical model and heuristic approach, *Appl. Math. Model.*, **80** (2020), 290–318. https://doi.org/10.1016/j.apm.2019.11.020
2. Y. Chang, Y. Cheng, U. Manzoor, J. Murray, A review of UAV autonomous navigation in GPS-denied environments, *Robot. Auton. Syst.*, **170** (2023), 104533. https://doi.org/10.1016/j.robot.2023.104533
3. T. Panigati, M. Zini, D. Striccoli, P. F. Giordano, D. Tonelli, M. P. Limongelli, et al., Drone-based bridge inspections: Current practices and future directions, *Autom. Constr.*, **173** (2025), 106101. https://doi.org/10.1016/j.autcon.2025.106101

4. S. Aggarwal, N. Kumar, Path planning techniques for unmanned aerial vehicles: a review, solutions, and challenges, *Comput. Commun.*, **149** (2020), 270–299. https://doi.org/10.1016/j.comcom.2019.10.014
5. A. Basiri, V. Mariani, G. Silano, M. Aatif, L. Iannelli, L. Glielmo, A survey on the application of path-planning algorithms for multi-rotor UAVs in precision agriculture, *J. Navigation*, **75** (2022), 364–383. https://doi.org/10.1017/S0373463321000825
6. Z. Zhang, J. Wu, J. Dai, C. He, Optimal path planning with modified A-Star algorithm for stealth unmanned aerial vehicles in 3D network radar environment, *Proc. Inst. Mech. Eng. Part G: J. Aerosp. Eng.*, **236** (2022), 72–81. https://doi.org/10.1177/09544100211007381
7. J. Fan, X. Chen, X. Liang, UAV trajectory planning based on bi-directional APF-RRT* algorithm with goal-biased, *Expert Syst. Appl.*, **213** (2023), 119137. https://doi.org/10.1016/j.eswa.2022.119137
8. N. Bashir, S. Boudjit, G. Dauphin, S. Zeadally, An obstacle avoidance approach for UAV path planning, *Simul. Model. Pract. Theory*, **129** (2023), 102815. https://doi.org/10.1016/j.simpat.2023.102815
9. X. Fu, J. Huang, Z. Jing, Complex switching dynamics and chatter alarm for aerial agents with artificial potential field method, *Appl. Math. Model.*, **107** (2022), 637–649. https://doi.org/10.1016/j.apm.2022.03.014
10. X. Li, L. Wang, H. Wang, L. Tao, X. Wang, A warm-started trajectory planner for fixed-wing unmanned aerial vehicle formation, *Appl. Math. Model.*, **122** (2023), 200–219. https://doi.org/10.1016/j.apm.2023.05.035
11. G. Hu, P. He, M. A. Salam, G. Wei, A novel framework for 4D UAV swarm path planning, *Appl. Math. Model.*, **150** (2026), 116383. https://doi.org/10.1016/j.apm.2025.116383
12. R. E. Precup, C. A. Bojan-Dragos, K. Gao, S. Cui, Problem setting for trajectory planning and cruise control of a connected autonomous electric bus in intersection scenarios with human-driven vehicles to optimize energy, comfort and tracking, *Rom. J. Inf. Sci. Technol.*, **28** (2025), 299–312. https://doi.org/10.59277/ROMJIST.2025.3.05
13. L. Gao, Y. Zhang, P. Liu, X. Ou, J. Cheng, Y. Zhu, Research on mathematical optimization-driven A* search, DWA improvement, and intelligent robot path planning, *AIMS Math.*, **10** (2025), 30879–30904. https://doi.org/10.3934/math.20251355
14. X. Chang, J. Yang, A golden ratio primal-dual algorithm for structured convex optimization, *J. Sci. Comput.*, **87** (2021), 47. https://doi.org/10.1007/s10915-021-01452-9
15. X. K. Chang, J. Yang, H. Zhang, Golden ratio primal-dual algorithm with linesearch, *SIAM J. Optim.*, **32** (2022), 1584–1613. https://doi.org/10.1137/21M1420319
16. A. Ait Saadi, A. Soukane, Y. Meraihi, A. B. Gabis, S. Mirjalili, A. Ramdane-Cherif, UAV path planning using optimization approaches: a survey, *Arch. Comput. Methods Eng.*, **29** (2022), 4233–4284. https://doi.org/10.1007/s11831-022-09742-7
17. Y. Chen, D. Pi, Y. Xu, Neighborhood global learning-based flower pollination algorithm and its application to unmanned aerial vehicle path planning, *Expert Syst. Appl.*, **170** (2021), 114505. https://doi.org/10.1016/j.eswa.2020.114505
18. C. Ye, P. Shao, S. Zhang, W. Wang, Three-dimensional unmanned aerial vehicle path planning utilizing artificial gorilla troops optimizer incorporating combined mutation and quadratic interpolation operators, *ISA Trans.*, **149** (2024), 196–216. https://doi.org/10.1016/j.isatra.2024.04.010

19. M. D. Phung, Q. P. Ha, Safety-enhanced UAV path planning with spherical vector-based particle swarm optimization, *Appl. Soft Comput.*, **107** (2021), 107376. https://doi.org/10.1016/j.asoc.2021.107376
20. J. Yang, F. Yan, J. Zhang, C. Peng, Hybrid chaos game and grey wolf optimization algorithms for UAV path planning, *Appl. Math. Model.*, **142** (2025), 115979. https://doi.org/10.1016/j.apm.2025.115979
21. G. Hu, F. Huang, A. Seyyedabbasi, G. Wei, Enhanced multi-strategy bottlenose dolphin optimizer for UAVs path planning, *Appl. Math. Model.*, **130** (2024), 243–271. https://doi.org/10.1016/j.apm.2024.03.001
22. W. Xie, X. Peng, Y. Liu, J. Zeng, L. Li, T. Eisaka, Conflict-free coordination planning for multiple automated guided vehicles in an intelligent warehousing system, *Simul. Model. Pract. Theory*, **134** (2024), 102945. https://doi.org/10.1016/j.simpat.2024.102945
23. H. Singh, S. Tyagi, P. Kumar, S. S. Gill, R. Buyya, Metaheuristics for scheduling of heterogeneous tasks in cloud computing environments: analysis, performance evaluation, and future directions, *Simul. Model. Pract. Theory*, **111** (2021), 102353. https://doi.org/10.1016/j.simpat.2021.102353
24. P. K. Panigrahi, S. K. Bisoy, Localization strategies for autonomous mobile robots: a review, *J. King Saud Univ. Comput. Inf. Sci.*, **34** (2022), 6019–6039. https://doi.org/10.1016/j.jksuci.2021.02.015
25. G. Hu, Y. Guo, G. Wei, L. Abualigah, Genghis Khan shark optimizer: A novel nature-inspired algorithm for engineering optimization, *Adv. Eng. Inform.*, **58** (2023), 102210. https://doi.org/10.1016/j.aei.2023.102210
26. P. Zhong, X. Wu, L. Zhu, A. Yang, A new APSO-SPC method for parameter identification problem with uncertainty caused by random measurement errors, *AIMS Math.*, **10** (2025), 3848–3865. https://doi.org/10.3934/math.2025179
27. I. A. Zamfirache, R. E. Precup, E. M. Petriu, Adaptive reinforcement learning-based control using proximal policy optimization and slime mould algorithm with experimental tower crane system validation, *Appl. Soft Comput.*, **160** (2024), 111687. https://doi.org/10.1016/j.asoc.2024.111687
28. E. K. Zavadskas, H. Dincer, S. Yuksel, S. Eti, Intelligent expert systems using molecular fuzzy genetic algorithms and multi-objective particle swarm optimization for circular-oriented project investments, *Rom. J. Inf. Sci. Technol.*, **28** (2025), 260–273. https://doi.org/10.59277/ROMJIST.2025.3.02
29. S. Meng, K. Chhea, S. Muy, J. R. Lee, Deep reinforcement learning and metaheuristic approaches to maximize downlink sum-rate for Internet of Things systems in non-orthogonal multiple access-based space-air-ground integrated networks, *Rom. J. Inf. Sci. Technol.*, **28** (2025), 327–340. https://doi.org/10.59277/ROMJIST.2025.4.02
30. A. Bouaouda, F. A. Hashim, Y. Sayouti, A. G. Hussien, Pied kingfisher optimizer: a new bio-inspired algorithm for solving numerical optimization and industrial engineering problems, *Neural Comput. Appl.*, **36** (2024), 15455–15513. https://doi.org/10.1007/s00521-024-09879-5
31. B. Hu, X. Zheng, W. Lai, EPKO: Enhanced pied kingfisher optimizer for numerical optimization and engineering problems, *Expert Syst. Appl.*, **278** (2025), 127416. https://doi.org/10.1016/j.eswa.2025.127416
32. B. Kanouni, A. Laib, S. Necaibia, A. Krama, J. M. Guerrero, Pied kingfisher optimizer for accurate parameter extraction in proton exchange membrane fuel cell, *Energy*, **325** (2025), 136079. https://doi.org/10.1016/j.energy.2025.136079

33. W. Qiu, C. Liu, B. Lin, X. Chen, D. Miao, Attribute reduction based on adaptive neighborhood rough sets and three-way pied kingfisher optimizer, *Expert Syst. Appl.*, **271** (2025), 126618. https://doi.org/10.1016/j.eswa.2025.126618
34. X. Wang, H. Liu, An improved pied kingfisher optimization algorithm based on multi-strategies for numerical and engineering problems, *Cluster Comput.*, **28** (2025), 979. https://doi.org/10.1007/s10586-025-05722-1

AIMS Press

©2026 the Author(s), licensee AIMS Press. This is an open access article distributed under the terms of the Creative Commons Attribution License (https://creativecommons.org/licenses/by/4.0)